(12) INTERNATIONAL APPLICATION PUBLISHED UNDER THE PATENT COOPERATION TREATY (PCT)

(19) World Intellectual Property Organization
International Bureau

(43) International Publication Date
10 July 2025 (10.07.2025)

WIPO | PCT

(10) International Publication Number
WO 2025/147348 A1

(51) International Patent Classification:
C12N 15/113 (2010.01) *A61P 17/02* (2006.01)
A61K 35/741 (2015.01) *A61K 31/223* (2006.01)
A61K 31/7088 (2006.01) *A61K 35/74* (2015.01)

(21) International Application Number:
PCT/US2024/058629

(22) International Filing Date:
05 December 2024 (05.12.2024)

(25) Filing Language: English

(26) Publication Language: English

(30) Priority Data:
63/617,598 04 January 2024 (04.01.2024) US

(71) Applicant: **THE JOHNS HOPKINS UNIVERSITY** [US/US]; 3400 N. Charles Street, Baltimore, Maryland 21218 (US).

(72) Inventors: **GARZA, Luis**; c/o The Johns Hopkins University, 3400 North Charles Street, Baltimore, Maryland 21218 (US). **WANG, Gaofeng**; c/o The Johns Hopkins University, 3400 North Charles Street, Baltimore, Maryland 21218 (US).

(74) Agent: **CHILDERS, Jeffrey W.**; 2275 Deming Way, Suite 310, Middleton, Wisconsin 53562 (US).

(81) Designated States *(unless otherwise indicated, for every kind of national protection available)*: AE, AG, AL, AM, AO, AT, AU, AZ, BA, BB, BG, BH, BN, BR, BW, BY, BZ, CA, CH, CL, CN, CO, CR, CU, CV, CZ, DE, DJ, DK, DM, DO, DZ, EC, EE, EG, ES, FI, GB, GD, GE, GH, GM, GT, HN, HR, HU, ID, IL, IN, IQ, IR, IS, IT, JM, JO, JP, KE, KG, KH, KN, KP, KR, KW, KZ, LA, LC, LK, LR, LS, LU, LY, MA, MD, MG, MK, MN, MU, MW, MX, MY, MZ, NA, NG, NI, NO, NZ, OM, PA, PE, PG, PH, PL, PT, QA, RO, RS, RU, RW, SA, SC, SD, SE, SG, SK, SL, ST, SV, SY, TH, TJ, TM, TN, TR, TT, TZ, UA, UG, US, UZ, VC, VN, WS, ZA, ZM, ZW.

(84) Designated States *(unless otherwise indicated, for every kind of regional protection available)*: ARIPO (BW, CV, GH, GM, KE, LR, LS, MW, MZ, NA, RW, SC, SD, SL, ST, SZ, TZ, UG, ZM, ZW), Eurasian (AM, AZ, BY, KG, KZ, RU, TJ, TM), European (AL, AT, BE, BG, CH, CY, CZ, DE, DK, EE, ES, FI, FR, GB, GR, HR, HU, IE, IS, IT, LT, LU, LV, MC, ME, MK, MT, NL, NO, PL, PT, RO, RS, SE, SI, SK, SM, TR), OAPI (BF, BJ, CF, CG, CI, CM, GA, GN, GQ, GW, KM, ML, MR, NE, SN, TD, TG).

Published:
— *with international search report (Art. 21(3))*

WO 2025/147348 A1

(54) Title: GLUTAMATE AND GLUTAMINE METABOLITES WITH OR WITHOUT dsRNA TO PROMOTE WOUND HEALING

(57) Abstract: Compositions and methods for promoting wound healing, treating photoaging, and/or inducing hair follicle regeneration, are disclosed.

GLUTAMATE AND GLUTAMINE METABOLITES WITH OR WITHOUT dsRNA TO PROMOTE WOUND HEALING

FEDERALLY SPONSORED RESEARCH OR DEVELOPMENT

This invention was made with government support under grant AR074846 awarded by the National Institutes of Health. The government has certain rights in the invention.

BACKGROUND

Tissue regeneration is an essential process for maintaining and protecting the skin barrier against infections, facilitating wound healing, and preserving the skins' aesthetic appearance. Burgeoning studies have shown that a critical determinant in the wound healing process is the homeostasis of the metabolome, as tissue injury induces metabolic changes influencing the regeneration process. A key aspect of the metabolic function influencing tissue regeneration is the commensal microbiome as in instances of pathologic conditions and trauma, the commensal microbiome has been shown to alter host metabolisms. For instance, exposure to ionizing radiation prompts intestinal bacteria like *Lachnospiraceae* and *Enterococcaceae* to enhance propionate and tryptophan metabolism, thereby improving host hematopoiesis and repairing intestinal damage. Similarly, transplant studies reveal that the intestinal microbiome of young mice positively impacts the intestinal health of older recipient mice through increased Firmicutes and *Lachnospiraceae*, promoting butyrate metabolism. Additionally, even in the skin, cutaneous microbes play a vital role in the host's metabolic regulation. Nevertheless, broad-spectrum topical antibiotics and treatments are conventionally used in the wound healing process. Studies have shown, however, that these treatments may impede wound healing, as they disrupt growth factors and impair cell migration and have a limited spectrum of effectiveness depending on the location and type of wound in addition to their potential to increase the risks of secondary infections. Consequently, there is a need for treatments that consider the dynamic changes in the microbiome and associated metabolic alterations during skin regeneration.

SUMMARY

In some aspects, the presently disclosed subject matter provides a method for

promoting wound healing, treating photoaging, and/or inducing hair follicle regeneration, the method comprising administering to a subject in need of treatment thereof, a therapeutically effective amount of one or more bacteria and/or one or more dsRNA sufficient to promote wound healing, treat photoaging, and/or induce hair follicle regeneration in the subject.

In certain aspects, the one or more bacteria are selected from *Staphylococcus*, *Pseudomonas*, and *Streptococcus*. In particular aspects, the one or more bacteria are *S. aureus*.

In certain aspects, administration of the one or more bacteria and/or one or more dsRNA: (a) induces local hypoxia and activates HIF1α signaling; (b) induces glutamine metabolism in one or more keratinocytes; and/or (c) activates downstream IL-1β signaling.

In certain aspects, the one or more bacteria and/or one of more dsRNA are applied topically to the wound and/or an area surrounding the wound.

In certain aspects, the wound is selected from a poor healing wound, a chronic wound, a diabetic chronic wound, a venous stasis chronic wound, an incised wound, and a tearing wound.

In certain aspects, the one or more bacteria and/or one or more dsRNA are administered via a pharmaceutical formulation.

In particular aspects, the pharmaceutical formulation comprises one or more of a solvent/liquid carrier, an emulsion, a cream, an ointment, a gel, a solid excipient, a polymer-based carrier, a liposome-based carrier, and a nanoparticle or microparticle.

In certain aspects, the pharmaceutical formulation comprises a bandage or a gauze.

In certain aspects, the pharmaceutical formulation further comprises one or more additional agents for promoting wound healing, treating photoaging, and/or inducing hair follicle regeneration.

In particular aspects, the one or more additional agents are selected from a retinoid, a vitamin, an anti-inflammatory agent, a steroid, a natural product, an antioxidant, and an analgesic.

In some aspects, the presently disclosed subject matter provides a method for promoting wound healing, treating photoaging, and/or inducing hair follicle regeneration, the method comprising administering to a subject in need of treatment thereof, a therapeutically effective amount of glutamine and/or glutamate with or without

one or more dsRNA sufficient to promote wound healing, treat photoaging, and/or induce hair follicle regeneration in the subject.

In certain aspects, administration of the glutamine and/or glutamate with or without one or more dsRNA: (a) induces local hypoxia and activates HIF1α signaling; (b) induces glutamine metabolism in one or more keratinocytes; and/or (c) activates downstream IL-1β signaling.

In certain aspects, the glutamine and/or glutamate with or without one or more dsRNA are applied topically to the wound and/or an area surrounding the wound.

In certain aspects, the wound is selected from a poor healing wound, a chronic wound, a diabetic chronic wound, a venous stasis chronic wound, an incised wound, and a tearing wound.

In certain aspects, the glutamine and/or glutamate with or without one or more dsRNA are administered via a pharmaceutical formulation.

In particular aspects, the pharmaceutical formulation comprises one or more of a solvent/liquid carrier, an emulsion, a cream, an ointment, a gel, a solid excipient, a polymer-based carrier, a liposome-based carrier, and a nanoparticle or microparticle.

In certain aspects, the pharmaceutical formulation comprises a bandage or a gauze.

In certain aspects, the pharmaceutical formulation further comprises one or more additional agents for promoting wound healing, treating photoaging, and/or inducing hair follicle regeneration.

In particular aspects, the one or more additional agents are selected from a retinoid, a vitamin, an anti-inflammatory agent, a steroid, a natural product, an antioxidant, and an analgesic.

Certain aspects of the presently disclosed subject matter having been stated hereinabove, which are addressed in whole or in part by the presently disclosed subject matter, other aspects will become evident as the description proceeds when taken in connection with the accompanying Examples and Drawings as best described herein below.

BRIEF DESCRIPTION OF THE FIGURES

The patent or application file contains at least one drawing executed in color. Copies of this patent or patent application publication with color drawing(s) will be provided by the Office upon request and payment of the necessary fee.

Having thus described the presently disclosed subject matter in general terms, reference will now be made to the accompanying Figures, which are not necessarily drawn to scale, and wherein:

FIG. 1A, FIG. 1B, FIG. 1C, FIG. 1D, FIG. 1E and FIG. 1F show that bacteria induced wound bed glutamine metabolism. (FIG. 1A) Energy metabolism score, calculated from microarray by principal components analysis (PCA) method, of GF (low WIHN) versus SPF (high WIHN) and PBS-treated (50 μL of WD3; low WIHN) versus *S. aureus*–treated mice (1×10^7 colony-forming units on WD3; high WIHN) using WD14 wound beds, the day of scab detachment (SD0). (FIG. 1B) Glutamine and glutamate gene signatures of microarrays from SD0 wound bed tissue of low WIHN strain (C57BL/6) versus high WIHN strain (B6/FVB/SJL) mice; GF versus SPF mice, and PBS-treated versus *S. aureus*–treated mice are shown. (FIG. 1C) mRNA expression of Gls and Gls2 in mice SD0 wound beds as detected by quantitative reverse transcription polymerase chain reaction (qRT-PCR). (FIG. 1D and FIG. 1E) GSEA of GF, SPF, PBS-treated, and *S. aureus*–treated mice glutamine and glutamate signatures based on SD0 microarrays. (FIG. 1F) On WD5 and SD0, glutamine and glutamate metabolite abundance in wound bed tissues as detected by mass spectrometry imaging (MSI; left) and quantification (right) of GF, SPF, PBS-treated, and *S. aureus*–treated mice. The magnified images indicate the wound bed, and the white dotted lines indicate the epidermal basement membrane. In quantification, each dot represents the expression of glutamine and glutamate as measured by mass spectrometry. Scatterplots and histogram graphs indicated means ± SEM; unpaired Student's t test was used to compare statistical difference. n = 3 to 4 independent animals per group. SA, *S. aureus*. NES, normalized enrichment score;

FIG. 2A, FIG. 2B, FIG. 2C, FIG. 2D, FIG. 2E, FIG. 2F, FIG. 2G and FIG. 2H show bacteria-induced keratinocyte IL-1β production via glutamine metabolism. (FIG. 2A) Detected by ELISA, glutamate expression of GF, SPF, PBS-treated, and *S. aureus*–treated mice at SD0. (FIG. 2B) Il-1β mRNA expression of mouse keratinocyte (MKC) treated with glutamine, CB839 (an inhibitor of glutamate production), or *S. aureus* as detected by qRT-PCR. DMSO, dimethyl sulfoxide. (FIG. 2C) As detected by ELISA, Il-1β expression of MKC treated with FX11, UK5099, CB839, glutamine, *S. aureus*, and *S. aureus* supernatant. (FIG. 2D) As detected by qRT-PCR and ELISA, Il-1β expression in mouse WD5 wound bed tissue treated with *S. aureus* and CB839. (FIG. 2E) IL-1β protein expression in human foreskin keratinocytes (HKC) treated with *S. aureus* and

CB839 as detected by immunofluorescence (IF). DAPI, 4′,6-diamidino-2-phenylindole. (FIG. 2F) Metabolism gene signatures in microarrays of unwounded and WD15 human skin. (FIG. 2G and FIG. 2H) Glutamine and glutamate expression in Vaseline-treated and Neosporin-treated human WD15 wound bed tissues as detected by MSI (FIG. 2H) and quantification (FIG. 2G) as in FIG. 1, with same statistical and graphing methods. n = 3 to 6 independent animals or independent human samples per group;

FIG. 3A, FIG. 3B, FIG. 3C and FIG. 3D demonstrate that glutamine metabolism induces the expression of stem cell markers and regenerative signaling *in vitro*. (FIG. 3A) The mRNA expression by qRT-PCR of regeneration markers Wnt7b, Shh, and stem cell marker Krt15 and differentiation marker Krt1 in CB839 treated mouse keratinocytes (MKC). (FIG. 3B) Wnt7b and Krt15 mRNA expression in CB839 treated Myd88–/– and IL-1β–/– MKC. (FIG. 3C) Immunofluorescence (left) and quantification (right) of CB839-treated human keratinocyte (HKC) stained for KRT15, active β-catenin (ABC), and KRT1 expression. (FIG. 3D) The mRNA expression of Shh, Wnt7b, and Krt1 of CB839 and mouse rmIL-1β–treated MKC. Statistics and graphing as in FIG. 1. n = 3 to 6 independent animals or independent human samples per group;

FIG. 4A, FIG. 4B , FIG. 4C, FIG. 4D, FIG. 4E , FIG. 4F and FIG. 4G show that glutamate is required for baseline and bacteria-induced WIHN. (FIG. 4A) WIHN of glutamine and CB839 treated (WD3) mice, compared to PBS controls, as detected by confocal scanning laser microscopy (CLSM) (top right), hematoxylin and eosin (H&E) staining (bottom right), and quantification (left). The red dashed squares indicate the regenerative hair follicles. (FIG. 4B) Glutamate production in SD0 mouse wound beds as measured by ELISA. (FIG. 4C) WIHN of *S. aureus*– and FX11-treated (WD3) mice, as detected by CSLM (right) and quantification (left). (FIG. 4D) WIHN of UK5099-treated (WD3) mice, as detected by CSLM (right) and quantification (left). (FIG. 4E) WIHN of *S. aureus*– and CB839-treated mice, as detected by CSLM (right) and quantification (left). (FIG. 4F) Glutamate and Il-1β production in *S. aureus*– and CB839-treated mice SD0 wound beds as measured by ELISA. (FIG. 4G) WIHN of glutamine-treated or untreated WT, Il-1β–/–, K14-Myd88–/–, and LysM-Myd88–/– mice (right) with quantification (left). Statistics and graphing as in FIG. 1. n = 3 to 7 independent animals per group;

FIG. 5A, FIG. 5B, FIG. 5C, FIG. 5D, FIG. 5E, FIG. 5F, FIG. 5G, FIG. 5H, FIG. 5I and FIG. 5J show bacteria-stimulated glutamine metabolism and IL-1β production through hypoxia-induced HIF signaling. (FIG. 5A and FIG. 5B) GSEA of DEGs (FIG.

5A) and relative mRNA (FIG. 5B) of hypoxia genes detected by microarray in SD0 wound bed of GF, SPF, PBS-treated, *S. aureus*–treated, low WIHN strain (C57BL/6), and high WIHN strain (B6/FVB/SJL) mice, as well as in Vaseline- and Neosporin-treated human wound bed. (FIG. 5C) qRT-PCR–determined mRNA expression of Hif-1α in SD0 skin of GF, SPF, PBS-treated, and *S. aureus*–, treated mice. (FIG. 5D) Il-1β mRNA expression by qRT-PCR under hypoxic conditions in MKC. (FIG. 5E) Il-1β expression in MKC treated with or without glutamine and Hif-1α siRNA, as detected by ELISA. (FIG. 5F) Glutamate expression of MKC treated with or without Hif-1α siRNA under hypoxic or normoxic conditions, as detected by ELISA. (FIG. 5G) Il-1β and Wnt7b expression of MKC are treated with or without Hif-1α siRNA under hypoxic or normoxic conditions, as detected by qRT-PCR. (FIG. 5H) Glutamate, Il-1β, Wnt7B, and Krt7 expression of *S. aureus*–induced MKC treated with or without Hif-1α siRNA, as detected by ELISA and qRT-PCR. Scr-siR indicates scramble siRNA. (FIG. 5I) WIHN of *S. aureus* and LW6 treated mice, as detected by CSLM (right) and quantification (left). The red dashed square indicate the regenerative hair follicles. (FIG. 5J) Glutamate and Il-1β expression of *S. aureus*– and LW6-treated (WD3) mice SD0 wound bed, as detected by ELISA. Graphing and statistics as in FIG. 1. n = 3 to 6 independent animals per group;

FIG. 6A, FIG. 6B, FIG. 6C, FIG. 6D, FIG. 6E, FIG. 6F, FIG. 6G, FIG. 6H and FIG. 6I, demonstrated that hypoxia and glutamine metabolism are elevated in wound center versus periphery in WIHN. (FIG. 6A and FIG. 6B) t-SNE plots visualization of WT mice SD0 wound center (high-WIHN, FIG. 6A) and SD0 wound periphery (non-WIHN, FIG. 6B) by scRNA-seq. Five mice were pooled per sample. (FIG. 6C) The overall number of cellular interactions in the wound center (top) or the periphery (bottom) at SD0 as detected by CellChat algorithm. Thicker lines indicate more interactions. (FIG. 6D) Specific cell-cell interaction patterns of IL-6 and IL-1 (left). Specific incoming signals of each cell type in the wound center and periphery at SD0 (right). Outgoing signals are shown in FIG. 14F. (FIG. 6E) The t-SNE plots clustered by all gene expression profiles (top) or just by hypoxia gene expression profiles (bottom) of SD0 keratinocytes. (FIG. 6F) GO enrichment analysis of keratinocytes in the wound center versus the periphery. (FIG. 6G) Scores for hypoxia, glutamine, and glutamate metabolism and IL-1 signaling calculated by PCA method in keratinocytes comparing wound center versus wound periphery. (FIG. 6H) The correlation of IL-1 signaling score and hypoxia score in keratinocytes as analyzed by Spearman correlation. The scores of

center and periphery of the wound are shown in red and blue, respectively. (FIG. 6I) GO enrichment analysis in the wound center keratinocytes with a high glutamate score (left) compared to those with a low glutamate score (right). The high and low glutamate scores were calculated using the PCA method as detailed in Materials and Methods. Box plot graphs indicated the value of minimum, first, quartile, median, third quartile, and maximum. Unless otherwise noted, statistics as in FIG. 1. NADH, reduced form of nicotinamide adenine dinucleotide;

FIG. 7A, FIG. 7B, FIG. 7C, FIG. 7D, FIG. 7E, FIG. 7F, FIG. 7G, FIG. 7H, FIG. 7I, FIG. 7J and FIG. 7K showed that hypoxia and glutamine metabolism correlate to hair follicle development in WIHN. (FIG. 7A) Heatmap for canonical keratinocyte marker genes in each cluster of the wound center from scRNA-seq of SD0 samples. (FIG. 7B) The t-SNE plot shows clustering of SD0 wound center keratinocytes subpopulations. (FIG. 7C) H&E, Col17a1, Cox-2, Ube2c, and Krt17 staining of SD0 wounds to establish location of basal1, basal2, proliferous, and HG keratinocytes. Scale bars, 50 μm. (FIG. 7D) Expression of HG marker genes to identify the HG cluster in t-SNE plots. (FIG. 7E) The scores for hypoxia, glutamine, and glutamate metabolism and IL-1 signaling in keratinocytes subpopulations. (FIG. 7F and FIG. 7G) Pseudotime analysis plotting the development pattern of basal, spinous, proliferative, and HG keratinocytes. (FIG. 7H) The heatmap of differentiation markers with pseudotime. (FIG. 7I) Pseudotime plot depicting the abundance of HG markers Krt17, Krt79, and Sox9 as divided by keratinocyte subpopulation. (FIG. 7J) Pseudotime analysis divided all keratinocytes (top) and HG (bottom) into six stages according to the developmental sequence; the different stages are indicated by different colors labeled A to F. (FIG. 7K) The gene expression scores for hypoxia, glutamine, and glutamate metabolism, and IL-1 signaling pathways as divided by HG developmental stage. Box plot graphs indicated the value of minimum, first, quartile, median, third quartile, and maximum. Statistics as in FIG. 1;

FIG. 8A, FIG. 8B, FIG. 8C, FIG. 8D, FIG. 8E, FIG. 8F, FIG. 8G, FIG. 8H, FIG. 8I, FIG. 8J and FIG. 8K demonstrate that bacteria promoted WIHN through keratinocyte-dependent IL-1βMyd88 and 16s-rRNA gene sequencing confirmed the expected changes in bacterial abundance. (FIG. 8A) Germ-free (GF) mice have the least WIHN, specific pathogen-free (SPF) mice have intermediate WIHN, and *S. aureus*-treated mice have the greatest WIHN. The regenerated hair follicles were detected by confocal scanning laser microscopy (right) and quantification (left). The red box indicates regenerated hair follicles (n = 5–6 independent animals per group). (FIG. 8B)

Immunofluorescence staining (upper) and quantification (lower) showed that βcatenin (top left) and Krt15 (top right) expressions were higher in *S. aureus*-treated mice than in control mice in wound bed epidermis at scab detachment day 0 (SD0) as normalized to adjacent normal skin. The dotted white line demarcates the boundary between the wound bed and normal tissue, and the white scale bar is 200 μm (n = 6 independent animals per group). (FIG. 8C, FIG. 8D) The relative abundance of taxonomic classifications at the genus level of 16S rRNA gene sequences of all species (FIG. 8C) and individual genera (FIG. 8D) from skin samples of GF, SPF, and *S. aureus*-infected mice (n = 5–14 independent animals per group). (FIG. 8E, FIG. 8F) The relative abundance of taxonomic classifications at the genus level of 16S rRNA gene sequences of all species (FIG. 8E) and individual genera (FIG. 8F) from skin samples of C57BL/6J (WT) mice, K14-Myd88 -/- mice, and IL-1β-/- mice (n = 4–5 independent animals per group). (FIG. 8G, FIG. 8H) WIHN in IL-1β-/- mice was significantly less than that in WT mice (FIG. 8G) and was not induced by *S. aureus* (FIG. 8H) (n = 5–6 independent animals per group). (FIG. 8I, FIG. 8J) WIHN in K14–Myd88-/- mice was significantly less than that in WT mice (FIG. 8I) and was not induced by *S. aureus* (FIG. 8J) (n = 5–7 independent animals per group). (FIG. 8K) The H&E staining images of GF, SPF, PBS-treated, and *S. aureus*-treated mice correspond to FIG. 1G and FIG. 11A. Representative data from 2–3 independent experiments are shown. Boxplot indicates the minimum, first quartile, median, third quartile, and maximum values. Scatterplots and bar graphs show the means ± SEM. A paired Student t-test was used to calculate the statistical difference (*$P < 0.05$, **$P < 0.01$, ***$P < 0.001$, ****$P < 0.0001$). NS indicates no significant difference;

FIG. 9A, FIG. 9B and FIG. 9C show that multiple metabolites do not correlate to bacterial load or wounding, as visualized by mass spectrometry imaging (MSI). (FIG. 9A) Spatial metabolomes of skin showed no significant difference in trace amine metabolism between GF, SPF, and *S. aureus*-treated mice at baseline (BL), WD5, or SD0. (FIG. 9B) Spatial metabolomes of skin show no significant difference in cholesterol metabolism between GF, SPF, and *S. aureus*-treated mice at BL, WD5, or SD0. (FIG. 9C) Spatial metabolomes of skin show no significant difference in triacylglycerol metabolism between GF, SPF, and *S. aureus*-treated mice at BL, WD5, or SD0;

FIG. 10A, FIG. 10B, FIG. 10C, FIG. 10D, FIG. 10E and FIG. 10F showed that multiple hair-related metabolites do not correlate to bacterial load wounding as visualized by mass spectrometry imaging (MSI). (FIG. 10A–10F) Spatial metabolomes

of skin showed no significant increase in gallic acid (FIG. 10A), αketoglutarate (FIG. 10B), inosine (FIG. 10C), inosine monophosphate (FIG. 10D), spermidine (FIG. 10E), or spermine (FIG. 10F) metabolism between GF, SPF, PBS-treated, and *S. aureus*-treated mice at baseline (BL), WD5, or SD0;

FIG. 11A and FIG. 11B show bacteria induced glutamine and glutamate in mouse and human wound bed, as visualized by mass spectrometry imaging (MSI). (FIG. 11A) On scab-detach day (SD) 0, glutamine, and glutamate metabolite abundance in wound bed tissues were detected by mass spectrometry imaging (MSI) and quantification (right) of GF, SPF, PBS-treated, and *S. aureus*-treated mice. The magnified images indicate the wound bed, and the white dotted line indicates the epidermal basement membrane. Each dot represents the expression of glutamine and glutamate measured by mass spectrometry as indicated by the scale bar. The corresponding hematoxylin and eosin (H&E) staining images of these samples are in FIG. 8K. (FIG. 11B) Glutamine and glutamate expression in Vaseline-treated and Neosporin-treated human WD-15 wound bed tissues as detected by MSI (Patient 2~4). The magnified images indicate the wound bed, and the white dotted line indicated the epidermal basement membrane. The signal strength of each dot was presented as a scale bar;

FIG. 12A, FIG. 12B, FIG. 12C, FIG. 12D, FIG. 12E, FIG. 12F, FIG. 12G, FIG. 12H, FIG. 12I, and FIG. 12J show that glutamine metabolism does not differ with bacterial load in unwounded skin and 16S-rRNA gene sequencing of skin microbes under different conditions. (FIG. 12A) MSI showed no significant difference in glutamine or glutamate metabolism between GF and SPF mouse skin at baseline (BL). (FIG. 12B) MSI showed no significant difference in glutamine or glutamate metabolism between PBS-treated and *S. aureus*-treated mouse skin at BL. (FIG. 12C) MSI showed no significant difference in glutamine or glutamate metabolism between Vaseline- and Neosporin-treated human skin at BL. (FIG. 12D–FIG. 12E) The relative abundance of taxonomic classifications at genus level of 16S rRNA gene sequence of all species (FIG. 12D), individual genera (FIG. 12E) in Vaseline- and Neosporin-treated human skin at baseline (pre-wounding; before product application) and wound bed (post-wounding; after product application) (n = 6 independent human samples per group). (FIG. 12F) Percentage of individual *Staphylococcus* species in Vaseline-and Neosporin-treated human skin at baseline and wound bed. (FIG. 12G) Schematic depicting keratinocyte energy metabolism and the key inhibitory targets. (FIG. 12H) The expression of glutamate in mouse keratinocytes decreased in glutamine deficient medium with or

without *S. aureus* stimulation (n = 3 independent animals per group). (FIG. 12I) qRT-PCR mRNA expression of Hif-1α confirmed the effectiveness of Hif-1α siRNA. (FIG. 12J) ELISA results showed that Slc1a7-siRNA reduced the expression of glutamate in mouse keratinocytes at baseline but not after *S. aureus* treatment (n = 3 independent animals per group). Scr-siR indicates scramble siRNA. Representative data from 2–3 independent experiments are shown. Bar graphs show the means ± SEM. A paired Student t-test was used to calculate the statistical difference (*P < 0.05, **P < 0.01, ***P < 0.001, ****P < 0.0001). NS indicates no significant difference;

FIG. 13A, FIG. 13B, FIG. 13C, FIG. 13D, FIG. 13E, FIG. 13F, FIG. 13G, FIG. 13H, FIG. 13I, and FIG. 13J illustrate that hypoxia and glutamine metabolism in keratinocytes during WIHN. (FIG. 13A) The t-SNE plot showed that combined gene expression profiles of normal skin, small wound at day 8 (SWD8), small wound day at 14 (SWD14), large wound center at day 14 (LWD14-center), and large wound periphery at day 14 (LWD14-periphery) from the GSE108677. The arrow indicates keratinocytes. Plots to the right describe canonical markers for each population. (FIG. 13B) Cells exhibited more interactions, particularly with growth factors, in the LWD14-center than in the LWD14-periphery. Thicker lines indicate more interactions. (FIG. 13C) Hypoxia, oxidative phosphorylation, and glutamine and glutamate metabolism scores calculated by PCA method were significantly higher in keratinocytes in the wound bed than in normal skin, and significantly higher in keratinocytes in the wound center (high-WIHN) than those in the wound periphery (non-WIHN). (FIG. 13D) The Spearman correlation coefficient between the IL-1 signal and hypoxia score was 0.69, with a P value < 2.2e-16. Scores for IL-1 signaling were positively correlated with the hypoxia score. (FIG. 13E) Gene ontology (GO) enrichment analysis of the DEGs in mice shows higher protein synthesis and mitochondrial energy metabolism and lower extracellular matrix organization categories in the wound bed center than in the periphery at WD14. (FIG. 13F) Pseudotime analysis showed that the keratinocytes of large wounds (high-WIHN) are less differentiated, and those of small wounds (non-WIHN) are more differentiated. (FIG. 13G) The heat map showed that basal stem cell markers DEGs in keratinocytes are expressed early, while suprabasal keratins are expressed later in pseudotime. (FIG. 13H) GO enrichment analysis shows that keratinocytes in the early stage of pseudotime have stronger proliferation, energy metabolism, and HIF1 signal expression. (FIG. 13I) Stem cell markers and developmental signals of keratinocytes decreased with pseudotime. (FIG. 13J) Hypoxia signal of keratinocytes decreased with pseudotime. Boxplots show

the minimum, first quartile, median, third quartile, and maximum values. A paired Student's t-test was used to calculate statistical differences (**P < 0.01, ***P < 0.001, ****P < 0.0001). NS indicates no significant difference; and

FIG. 14A, FIG. 14B, FIG. 14C, FIG. 14D, FIG. 14E, FIG. 14F, FIG. 14G, FIG. 14H, FIG. 14I, FIG. 14J, FIG. 14K and FIG. 14L showed that single cell RNA-seq analysis of mouse wound bed in self-test dataset. (FIG. 14A, FIG. 14B) The t-SNE plot showed gene expression profiles of the SD0 wound center. A total of 24 clusters were automatically assembled. Different clusters of cells are shown in different colors. Marker gene expression in different clusters is shown in FIG. 14B. (FIG. 14C, FIG. 14D) The t-SNE plot showed gene expression profiles of the SD0 wound periphery. A total of 25 clusters were automatically assembled. Different clusters of cells are shown in different colors. Marker gene expression in different clusters is shown in FIG. 14D. (FIG. 14E) The strength of interactions between fibroblasts and keratinocytes and among keratinocytes was stronger in the wound center than in the wound periphery at SD0. (FIG. 14F) Specific outgoing signals of each cell type in the SD0 center and periphery. The IL-1 marked by the red arrow appears only in the center and is missing from the periphery. (FIG. 14G) The expression of chemokines and inflammatory factors in various cell types within the wound center and periphery. (FIG. 14H) The t-SNE plot is based on oxidative phosphorylation gene expression profiles in SD0 keratinocytes. The keratinocytes in different positions are shown in different colors. The keratinocytes in the center are not separated from those in the periphery. (FIG. 14I) Proteomics data showed that the scores for retinoic acid metabolism, glutamine metabolism, and glutathione metabolism were higher in the wound bed center (red arrows). In contrast, scores for fatty acid and glucose metabolism were higher in the wound bed periphery (black arrows). (FIG. 14J) Proteomic data showed that the scores for hypoxia, glutamine metabolism, glutamate metabolism, and IL-1 signaling were significantly higher in keratinocytes in the wound center (WIHN) than in those in the wound periphery (non-WIHN). The higher keratinocyte differentiation score in the wound periphery confirms the accuracy of the proteomic analysis. *P < 0.05. (FIG. 14K) Specific incoming and outgoing signals of each keratinocyte subtype in the wound center and periphery at SD0. The red arrows indicate that keratinocytes receive more IL-6 and IL-1 signals than other cell types. (FIG. 14L) Schematic illustrated that the kin commensal microbiome induces hypoxia in the wound microenvironment and activates HIF1α signaling, promoting glutamine metabolism in keratinocytes, thus activating downstream IL-1β signaling to

promote WIHN.

DETAILED DESCRIPTION

The presently disclosed subject matter now will be described more fully hereinafter with reference to the accompanying Figures, in which some, but not all embodiments of the inventions are shown. Like numbers refer to like elements throughout. The presently disclosed subject matter may be embodied in many different forms and should not be construed as limited to the embodiments set forth herein; rather, these embodiments are provided so that this disclosure will satisfy applicable legal requirements. Indeed, many modifications and other embodiments of the presently disclosed subject matter set forth herein will come to mind to one skilled in the art to which the presently disclosed subject matter pertains having the benefit of the teachings presented in the foregoing descriptions and the associated Figures. Therefore, it is to be understood that the presently disclosed subject matter is not to be limited to the specific embodiments disclosed and that modifications and other embodiments are intended to be included within the scope of the appended claims.

In some embodiments, the presently disclosed subject matter provides a method for promoting wound healing, treating photoaging, and/or inducing hair follicle regeneration, the method comprising administering to a subject in need of treatment thereof, a therapeutically effective amount of one or more bacteria and/or one or more double-stranded RNA sufficient to promote wound healing, treat photoaging, and/or induce hair follicle regeneration in the subject.

In certain embodiments, the wound is selected from a poor healing wound, a poor healing wound, a chronic wound, a diabetic chronic wound, a venous stasis chronic wounds an incised wound, and a tearing wound.

As used herein, the term "photoaging" refers to skin aging, including premature skin aging, resulting from, for example, prolonged and/or repeated exposure to solar radiation, including ultraviolet radiation, such as UV-A and UV-B radiation. Photoaging also can be referred to as "extrinsic aging" or "dermatoheliosis." The cumulative detrimental effects of photoaging can include wrinkles and dyspigmentation, including dark spots. Other common symptoms of photoaging include, but are not limited to, telangiectasias (i.e., spider veins), leathery and/or lax (loose) skin, solar lentigines (e.g., age spots, for example on the face and hands), and actinic keratosis (i.e., rough, scaly patches or bumps on the skin, which can be pre-cancerous).

In certain embodiments, the one or more bacteria are selected from *Staphylococcus*, *Pseudomonas*, and *Streptococcus*. In particular embodiments, the one or more bacteria are *S. aureus*.

In certain embodiments, administration of the one or more bacteria and/or one or more dsRNA: (a) induces local hypoxia and activates HIF1α signaling; (b) induces glutamine metabolism in one or more keratinocytes; and/or (c) activates downstream IL-1β signaling.

In certain embodiments, the one or more bacteria and/or one of more dsRNA are applied topically to the wound and/or an area surrounding the wound.

In certain embodiments, the one or more bacteria and/or one or more dsRNA are administered via a pharmaceutical formulation.

In particular embodiments, the pharmaceutical formulation comprises one or more of a solvent/liquid carrier, an emulsion, a cream, an ointment, a gel, a solid excipient, a polymer-based carrier, a liposome-based carrier, and a nanoparticle or microparticle.

In further embodiments, the pharmaceutical formulation comprises a bandage or a gauze.

In certain embodiments, the pharmaceutical formulation further comprises one or more additional agents for promoting wound healing, treating photoaging, and/or inducing hair follicle regeneration.

In particular embodiments, the one or more additional agents are selected from a retinoid, a vitamin, an anti-inflammatory agent, a steroid, a natural product, an antioxidant, and an analgesic.

In some embodiments, the presently disclosed subject matter provides a method for promoting wound healing, treating photoaging, and/or inducing hair follicle regeneration, the method comprising administering to a subject in need of treatment thereof, a therapeutically effective amount of glutamine and/or glutamate with or without one or more double-stranded RNA sufficient to promote wound healing, treat photoaging, and/or induce hair follicle regeneration in the subject.

In certain embodiments, administration of the glutamine and/or glutamate with or without one or more dsRNA: (a) induces local hypoxia and activates HIF1α signaling; (b) induces glutamine metabolism in one or more keratinocytes; and/or (c) activates downstream IL-1β signaling.

In certain embodiments, the glutamine and/or glutamate with or without one or more dsRNA are applied topically to the wound and/or an area surrounding the wound.

In certain embodiments, the glutamine and/or glutamate with or without one or more dsRNA are administered via a pharmaceutical formulation.

In particular embodiments, the pharmaceutical formulation comprises one or more of a solvent/liquid carrier, an emulsion, a cream, an ointment, a gel, a solid excipient, a polymer-based carrier, a liposome-based carrier, and a nanoparticle or microparticle.

In further embodiments, the pharmaceutical formulation comprises a bandage or a gauze.

In certain embodiments, the pharmaceutical formulation further comprises one or more additional agents for promoting wound healing, treating photoaging, and/or inducing hair follicle regeneration.

In particular embodiments, the one or more additional agents are selected from a retinoid, a vitamin, an anti-inflammatory agent, a steroid, a natural product, an antioxidant, and an analgesic.

As used herein, the term "treating" can include reversing, alleviating, inhibiting the progression of, preventing, or reducing the likelihood of the disease, disorder, or condition to which such term applies, or one or more symptoms or manifestations of such disease, disorder, or condition. Preventing refers to causing a disease, disorder, condition, or symptom or manifestation of such, or worsening of the severity of such, not to occur. Accordingly, the presently disclosed compounds can be administered prophylactically to prevent or reduce the incidence or recurrence of the disease, disorder, or condition.

The "subject" treated by the presently disclosed methods in their many embodiments is desirably a human subject, although it is to be understood that the methods described herein are effective with respect to all vertebrate species, which are intended to be included in the term "subject." Accordingly, a "subject" can include a human subject for medical purposes, such as for the treatment of an existing condition or disease or the prophylactic treatment for preventing the onset of a condition or disease, or an animal subject for medical, veterinary purposes, or developmental purposes. Suitable animal subjects include mammals including, but not limited to, primates, e.g., humans, monkeys, apes, and the like; bovines, e.g., cattle, oxen, and the like; ovines, e.g., sheep and the like; caprines, e.g., goats and the like; porcines, e.g., pigs, hogs, and the like; equines, e.g., horses, donkeys, zebras, and the like; felines, including wild and domestic cats; canines, including dogs; lagomorphs, including rabbits, hares, and the

like; and rodents, including mice, rats, and the like. An animal may be a transgenic animal. In some embodiments, the subject is a human including, but not limited to, fetal, neonatal, infant, juvenile, and adult subjects. Further, a "subject" can include a patient afflicted with or suspected of being afflicted with a condition or disease. Thus, the terms "subject" and "patient" are used interchangeably herein. The term "subject" also refers to an organism, tissue, cell, or collection of cells from a subject.

In general, the "effective amount" of an active agent or drug delivery device refers to the amount necessary to elicit the desired biological response. As will be appreciated by those of ordinary skill in this art, the effective amount of an agent or device may vary depending on such factors as the desired biological endpoint, the agent to be delivered, the makeup of the pharmaceutical composition, the target tissue, and the like.

The term "combination" is used in its broadest sense and means that a subject is administered at least two agents, more particularly a compound disclosed herein and at least one other therapeutic agent. More particularly, the term "in combination" refers to the concomitant administration of two (or more) active agents for the treatment of a, e.g., single disease state. As used herein, the active agents may be combined and administered in a single dosage form, may be administered as separate dosage forms at the same time, or may be administered as separate dosage forms that are administered alternately or sequentially on the same or separate days. In one embodiment of the presently disclosed subject matter, the active agents are combined and administered in a single dosage form. In another embodiment, the active agents are administered in separate dosage forms (e.g., wherein it is desirable to vary the amount of one but not the other). The single dosage form may include additional active agents for the treatment of the disease state.

Further, the compounds disclosed herein can be administered alone or in combination with adjuvants that enhance stability of the compounds, alone or in combination with one or more therapeutic agents, facilitate administration of pharmaceutical compositions containing them in certain embodiments, provide increased dissolution or dispersion, increase inhibitory activity, provide adjunct therapy, and the like, including other active ingredients. Advantageously, such combination therapies utilize lower dosages of the conventional therapeutics, thus avoiding possible toxicity and adverse side effects incurred when those agents are used as monotherapies.

The timing of administration of a compound disclosed herein and at least one additional therapeutic agent can be varied so long as the beneficial effects of the

combination of these agents are achieved. Accordingly, the phrase "in combination with" refers to the administration of a compound described herein and at least one additional therapeutic agent either simultaneously, sequentially, or a combination thereof. Therefore, a subject administered a combination of a compound described herein and at least one additional therapeutic agent can receive a compound and at least one additional therapeutic agent at the same time (i.e., simultaneously) or at different times (i.e., sequentially, in either order, on the same day or on different days), so long as the effect of the combination of both agents is achieved in the subject.

When administered sequentially, the agents can be administered within 1, 5, 10, 30, 60, 120, 180, 240 minutes or longer of one another. In other embodiments, agents administered sequentially, can be administered within 1, 5, 10, 15, 20 or more days of one another. Where the compound described herein and at least one additional therapeutic agent are administered simultaneously, they can be administered to the subject as separate pharmaceutical compositions, each comprising either a compound or at least one additional therapeutic agent, or they can be administered to a subject as a single pharmaceutical composition comprising both agents.

When administered in combination, the effective concentration of each of the agents to elicit a particular biological response may be less than the effective concentration of each agent when administered alone, thereby allowing a reduction in the dose of one or more of the agents relative to the dose that would be needed if the agent was administered as a single agent. The effects of multiple agents may, but need not be, additive or synergistic. The agents may be administered multiple times.

In some embodiments, when administered in combination, the two or more agents can have a synergistic effect. As used herein, the terms "synergy," "synergistic," "synergistically" and derivations thereof, such as in a "synergistic effect" or a "synergistic combination" or a "synergistic composition" refer to circumstances under which the biological activity of a combination of a compound described herein and at least one additional therapeutic agent is greater than the sum of the biological activities of the respective agents when administered individually.

Synergy can be expressed in terms of a "Synergy Index (SI)," which generally can be determined by the method described by F. C. Kull et al., Applied Microbiology 9, 538 (1961), from the ratio determined by:

$$Q_a/Q_A + Q_b/Q_B = \text{Synergy Index (SI)}$$

wherein:

Q_A is the concentration of a component A, acting alone, which produced an end point in relation to component A;

Q_a is the concentration of component A, in a mixture, which produced an end point;

Q_B is the concentration of a component B, acting alone, which produced an end point in relation to component B; and

Q_b is the concentration of component B, in a mixture, which produced an end point.

Generally, when the sum of Q_a/Q_A and Q_b/Q_B is greater than one, antagonism is indicated. When the sum is equal to one, additivity is indicated. When the sum is less than one, synergism is demonstrated. The lower the SI, the greater the synergy shown by that particular mixture. Thus, a "synergistic combination" has an activity higher that what can be expected based on the observed activities of the individual components when used alone. Further, a "synergistically effective amount" of a component refers to the amount of the component necessary to elicit a synergistic effect in, for example, another therapeutic agent present in the composition.

Depending on the specific conditions being treated, the "agent(s)" may be formulated into liquid or solid dosage forms and administered systemically or locally. The agents may be delivered, for example, in a timed- or sustained-slow release form as is known to those skilled in the art. Techniques for formulation and administration may be found in Remington: The Science and Practice of Pharmacy (20^{th} ed.) Lippincott, Williams & Wilkins (2000). Suitable routes may include oral, buccal, by inhalation spray, sublingual, rectal, transdermal, vaginal, transmucosal, nasal or intestinal administration; parenteral delivery, including intramuscular, subcutaneous, intramedullary injections, as well as intrathecal, direct intraventricular, intravenous, intra-articular, intra-sternal, intra-synovial, intra-hepatic, intralesional, intracranial, intraperitoneal, intranasal, or intraocular injections or other modes of delivery.

For injection, the agents of the disclosure may be formulated and diluted in aqueous solutions, such as in physiologically compatible buffers such as Hank's solution, Ringer's solution, or physiological saline buffer. For such transmucosal administration, penetrants appropriate to the barrier to be permeated are used in the formulation. Such penetrants are generally known in the art.

Use of pharmaceutically acceptable inert carriers to formulate the compounds herein disclosed for the practice of the disclosure into dosages suitable for systemic administration is within the scope of the disclosure. With proper choice of carrier and suitable manufacturing practice, the compositions of the present disclosure, in particular,

those formulated as solutions, may be administered parenterally, such as by intravenous injection. The compounds can be formulated readily using pharmaceutically acceptable carriers well known in the art into dosages suitable for oral administration. Such carriers enable the compounds of the disclosure to be formulated as tablets, pills, capsules, liquids, gels, syrups, slurries, suspensions, and the like, for oral ingestion by a subject (e.g., patient) to be treated.

For nasal or inhalation delivery, the agents of the disclosure also may be formulated by methods known to those of skill in the art, and may include, for example, but not limited to, examples of solubilizing, diluting, or dispersing substances, such as saline; preservatives, such as benzyl alcohol; absorption promoters; and fluorocarbons.

In particular embodiments, the compound disclosed herein is administered intranasally in a form selected from the group consisting of a nasal spray, a nasal drop, a powder, a granule, a cachet, a tablet, an aerosol, a paste, a cream, a gel, an ointment, a salve, a foam, a paste, a lotion, a cream, an oil suspension, an emulsion, a solution, a patch, and a stick. As used herein, the term administrating via an "intranasal route" refers to administering by way of the nasal structures.

Pharmaceutical compositions suitable for use in the present disclosure include compositions wherein the active ingredients are contained in an effective amount to achieve its intended purpose. Determination of the effective amounts is well within the capability of those skilled in the art, especially in light of the detailed disclosure provided herein. Generally, the compounds according to the disclosure are effective over a wide dosage range. For example, in the treatment of adult humans, dosages from 0.01 to 1000 mg, from 0.5 to 100 mg, from 1 to 50 mg per day, and from 5 to 40 mg per day are examples of dosages that may be used. A non-limiting dosage is 10 to 30 mg per day. The exact dosage will depend upon the route of administration, the form in which the compound is administered, the subject to be treated, the body weight of the subject to be treated, the bioavailability of the compound(s), the adsorption, distribution, metabolism, and excretion (ADME) toxicity of the compound(s), and the preference and experience of the attending physician.

In addition to the active ingredients, these pharmaceutical compositions may contain suitable pharmaceutically acceptable carriers comprising excipients and auxiliaries which facilitate processing of the active compounds into preparations which can be used pharmaceutically. The preparations formulated for oral administration may be in the form of tablets, dragees, capsules, or solutions.

Pharmaceutical preparations for oral use can be obtained by combining the active compounds with solid excipients, optionally grinding a resulting mixture, and processing the mixture of granules, after adding suitable auxiliaries, if desired, to obtain tablets or dragee cores. Suitable excipients are, in particular, fillers such as sugars, including lactose, sucrose, mannitol, or sorbitol; cellulose preparations, for example, maize starch, wheat starch, rice starch, potato starch, gelatin, gum tragacanth, methyl cellulose, hydroxypropylmethyl-cellulose, sodium carboxymethyl-cellulose (CMC), and/or polyvinylpyrrolidone (PVP: povidone). If desired, disintegrating agents may be added, such as the cross-linked polyvinylpyrrolidone, agar, or alginic acid or a salt thereof such as sodium alginate.

Dragee cores are provided with suitable coatings. For this purpose, concentrated sugar solutions may be used, which may optionally contain gum arabic, talc, polyvinylpyrrolidone, carbopol gel, polyethylene glycol (PEG), and/or titanium dioxide, lacquer solutions, and suitable organic solvents or solvent mixtures. Dye-stuffs or pigments may be added to the tablets or dragee coatings for identification or to characterize different combinations of active compound doses.

Pharmaceutical preparations that can be used orally include push-fit capsules made of gelatin, as well as soft, sealed capsules made of gelatin, and a plasticizer, such as glycerol or sorbitol. The push-fit capsules can contain the active ingredients in admixture with filler such as lactose, binders such as starches, and/or lubricants such as talc or magnesium stearate and, optionally, stabilizers. In soft capsules, the active compounds may be dissolved or suspended in suitable liquids, such as fatty oils, liquid paraffin, or liquid polyethylene glycols (PEGs). In addition, stabilizers may be added.

Further, one of ordinary skill in the art will recognize that the presently disclosed compounds, and pharmaceutical compositions thereof, include pharmaceutically acceptable salts. Pharmaceutically acceptable salts are generally well known to those of ordinary skill in the art, and include salts of active compounds that can be prepared with relatively nontoxic acids or bases, depending on the particular substituent moieties found on the compounds described herein. The parent form of the compound can differ from the various salt forms in certain physical properties, such as solubility, and the like.

When compounds of the present disclosure contain relatively acidic functionalities, base addition salts can be obtained by contacting the neutral form of such compounds with a sufficient amount of the desired base, either neat or in a suitable inert solvent or by ion exchange, whereby one basic counterion (base) in an ionic complex is

substituted for another. Examples of pharmaceutically acceptable base addition salts include sodium, potassium, calcium, ammonium, organic amino, magnesium, and the like.

When compounds of the present disclosure contain relatively basic functionalities, acid addition salts can be obtained by contacting the neutral form of such compounds with a sufficient amount of the desired acid, either neat or in a suitable inert solvent or by ion exchange, whereby one acidic counterion (acid) in an ionic complex is substituted for another. Examples of pharmaceutically acceptable acid addition salts include those derived from inorganic acids, organic acids, and amino acids. See, for example, Berge et al, "Pharmaceutical Salts", Journal of Pharmaceutical Science, 1977, 66, 1-19). Compounds containing both basic and acidic functionalities allow such compounds to be converted into either base or acid addition salts.

Accordingly, pharmaceutically acceptable salts suitable for use with the presently disclosed subject matter include, by way of example but not limitation, acetate, arginate, benzenesulfonate, benzoate, bicarbonate, bitartrate, bromide, calcium edetate, camsylate, carbonate, monohydrogencarbonate, citrate, edetate, edisylate, estolate, esylate, fumarate, galactonate, gluceptate, gluconate, glutamate, glycollylarsanilate, hexylresorcinate, hydrabamine, hydriodic, hydrobromide, hydrochloride, hydroxynaphthoate, iodide, isethionate, isobutyrate, lactate, lactobionate, malate, maleate, malonate, mandelate, mesylate, methanesulfonate, mucate, napsylate, nitrate, pamoate (embonate), pantothenate, phosphate, phthalate, diphosphate, monohydrogen phosphate, dihydrogen phosphate, polygalacturonate, propionate, salicylate, stearate, subacetate, suberate, succinate, sulfate, monohydrogensulfate, tannate, tartrate, including (+)-tartrates, (-)-tartrates, and mixtures thereof including racemic mixtures, teoclate, p-toluenesulfonate and trifluoroacetate. Other pharmaceutically acceptable salts may be found in, for example, Remington: The Science and Practice of Pharmacy (20th ed.) Lippincott, Williams & Wilkins (2000).

Unless otherwise noted, the chemical definitions provided immediately herein below are intended to comply with IUPAC. Compendium of Chemical Terminology, 2nd ed. (the "Gold Book"). Compiled by A. D. McNaught and A. Wilkinson. Blackwell Scientific Publications, Oxford (1997).

Following long-standing patent law convention, the terms "a," "an," and "the" refer to "one or more" when used in this application, including the claims. Thus, for example, reference to "a subject" includes a plurality of subjects, unless the context

clearly is to the contrary (e.g., a plurality of subjects), and so forth.

Throughout this specification and the claims, the terms "comprise," "comprises," and "comprising" are used in a non-exclusive sense, except where the context requires otherwise. Likewise, the term "include" and its grammatical variants are intended to be non-limiting, such that recitation of items in a list is not to the exclusion of other like items that can be substituted or added to the listed items.

For the purposes of this specification and appended claims, unless otherwise indicated, all numbers expressing amounts, sizes, dimensions, proportions, shapes, formulations, parameters, percentages, quantities, characteristics, and other numerical values used in the specification and claims, are to be understood as being modified in all instances by the term "about" even though the term "about" may not expressly appear with the value, amount or range. Accordingly, unless indicated to the contrary, the numerical parameters set forth in the following specification and attached claims are not and need not be exact, but may be approximate and/or larger or smaller as desired, reflecting tolerances, conversion factors, rounding off, measurement error and the like, and other factors known to those of skill in the art depending on the desired properties sought to be obtained by the presently disclosed subject matter. For example, the term "about," when referring to a value can be meant to encompass variations of, in some embodiments, ± 100% in some embodiments ± 50%, in some embodiments ± 20%, in some embodiments ± 10%, in some embodiments ± 5%, in some embodiments ±1%, in some embodiments ± 0.5%, and in some embodiments ± 0.1% from the specified amount, as such variations are appropriate to perform the disclosed methods or employ the disclosed compositions.

Further, the term "about" when used in connection with one or more numbers or numerical ranges, should be understood to refer to all such numbers, including all numbers in a range and modifies that range by extending the boundaries above and below the numerical values set forth. The recitation of numerical ranges by endpoints includes all numbers, e.g., whole integers, including fractions thereof, subsumed within that range (for example, the recitation of 1 to 5 includes 1, 2, 3, 4, and 5, as well as fractions thereof, e.g., 1.5, 2.25, 3.75, 4.1, and the like) and any range within that range.

EXAMPLES

The following Examples have been included to provide guidance to one of ordinary skill in the art for practicing representative embodiments of the presently

disclosed subject matter. In light of the present disclosure and the general level of skill in the art, those of skill can appreciate that the following Examples are intended to be exemplary only and that numerous changes, modifications, and alterations can be employed without departing from the scope of the presently disclosed subject matter. The synthetic descriptions and specific examples that follow are only intended for the purposes of illustration and are not to be construed as limiting in any manner to make compositions of the disclosure by other methods.

EXAMPLE 1

1.1 Overview

The microbiome plays an important role in homeostatic tissue maintenance, healing, and regeneration. Wang et al., 2021; Abo et al., 2020; Wu et al., 2020. Studies have shown that in pathologic conditions and trauma, commensal microbiomes alter host metabolisms. Liu et al., 2020; He et al., 2020. For example, when exposed to ionizing radiation, the intestinal bacteria *Lachnospiraceae* and *Enterococcaceae* can promote propionate and tryptophan metabolism, improving host hematopoiesis and repairing intestinal damage. Guo et al., 2020. Likewise, in transplant studies, the intestinal microbiome of young mice enhances the intestinal health of old recipient mice through increased Firmicutes and *Lachnospiraceae* and the promotion of butyrate metabolism. Kundu et al., 2019. In the skin, cutaneous microbes also are essential for the host's metabolic regulation. Roux et al., 2021; Chen et al., 2021.

Commensal microbiome has been shown to have a positive effect on skin regeneration, specifically through interleukin-1β (IL-1β) signaling. Wang et al., 2021. When skin injury induces inflammation, immune cells—mainly macrophages—release IL- 1β to stimulate wound-induced hair follicle neogenesis (WIHN). Keratinocytes also express high levels of IL-1β in inflammatory skin diseases or trauma. Cai et al., 2018; Salgado et al., 2012.

Glutamine also is an important metabolite for the transcription and production of IL-1β, as previous studies on energy metabolism have shown. Rodriguez et al., 2019; Tannahill et al., 2013. Furthermore, glutamine metabolism modulated by mammalian target of rapamycin complex 2 (mTORC2) is important for repopulating hair follicle stem cells (HFSCs) after mobilization at the onset of anagen. Kim et al., 2020. Similarly, previous studies have shown that glutamine is an important energy source for hair follicles. Williams et al., 1993. It is contemplated that glutamine metabolism approach finds use in hair follicle regeneration by promoting the production of hair follicle

neogenic signals and by directly activating HFSCs.

Without wishing to be bound to any one particular theory, it was thought that skin-resident bacteria may link glutamine to skin and hair follicle regeneration by producing local hypoxia in wounds. For example, *Staphylococcus aureus* induces keratinocyte IL-1β production by hypoxia-inducible factor-1α (HIF-1α) signaling. Wickersham et al., 2017. The HIF-1α signal plays an important regulatory role in tissue hypoxia to maintain the homeostasis of the microenvironment, especially in the regulation of energy metabolism. McGettrick et al., 2020; Kim et al., 2006. Local oxygen concentration can directly affect the self-renewal and differentiation of stem cells. Hematopoietic stem cells, neural stem cells, and human placental cytotrophoblast cells benefit from living in a low-oxygen environment Schipani et al., 2001; Genbacev et al., 1997. Hypoxia promotes long-term preservation and maintenance of stem cells, including HFSCs. Kim et al., 2020; Flores et al., 2017. During the course of proliferation and metabolic activity, *S. aureus* contributes to hypoxia by consuming nutrients and oxygen in the microenvironment, Lone et al., 2015, showing a path through which skin flora can be used to regulate metabolism to promote regeneration.

In some embodiments, a goal of this Example was to examine and unify the elements of the coherent physiologic model that tests the role of metabolism in the microbiome promotion of regeneration in mice and humans. To do so, spatial metabolomics and bioinformatics was used to systematically screen the wound microenvironment under different bacterial loads. It was shown that glutamine metabolism positively correlates with bacterial load. It also was demonstrated that *S. aureus* activates HIF-1α signaling by inducing tissue hypoxia, with concomitant increase in keratinocyte glutamine metabolism and production of IL-1β to promote regeneration. Furthermore, the reduction of commensal bacteria reduces glutamine levels and retards wound healing in human subjects. These findings showed a conserved proregenerative metabolic program induced by skin flora with important therapeutic implications.

1.2 Materials and Methods

1.2.1 Animals

The backgrounds of all mice are based on C57BL/6J. The GF mice were provided and managed by the Germ-Free laboratory of the Johns Hopkins Bloomberg School of Public Health. SPF mice were provided and housed by the animal facility of the Johns Hopkins School of Medicine. C57BL/6J, LysM-cre [B6.129P2-Lyz2tm1(cre)Ifo/J], and Myd88fl/Fl [B6.129P2(SJL)-Myd88tm1- Defr/J] mice were

obtained from The Jackson Laboratory. LysM-cre mice were crossed with MyD88fl/fl mice to obtain the LysM-cre × MyD88fl/Fl mouse strain. K14-MyD88–/– mice were provided by N. Archer (Johns Hopkins Medical Institutions). Il-1β–/– mice were provided by Y. Iwakura (University of Tokyo) and obtained from the Johns Hopkins University School of Medicine through a material transfer agreement. DNA was extracted from mouse tails to confirm the genotype via PCR. All mouse breeding and experiments were approved by the Johns Hopkins Animal Care and Use Committee and based on Institutional Animal Care and Use Committee protocol MO17M298 (noninfection experiment) and MO25M421 (infection experiment).

1.2.2 Human samples

The human skin samples were acquired according to the Helsinki Principles after volunteers provided informed consent. All study activities were overseen by the Johns Hopkins Institutional Review Board under NA_00033375. Discarded neonatal foreskin from Johns Hopkins Hospital was collected for keratinocyte isolation and culture as described previously. Kim et al., 2019. Briefly, 32 skin samples from 10 adult volunteers who had not used topical antibiotics within 7 days or systemic antibiotics within 6 months were included. Volunteers were asked not to wash for 24 hours before the start of the study and to refrain from using antibacterial soaps during the study. Twenty-four skin samples from six volunteers were collected for transcriptome sequencing and 16S ribosomal RNA (rRNA) sequence (age range:18 to 53 years old; three males and three females; two Caucasian, one Black, two Hispanic, and one Asian). On day 0 (D0), full-thickness punch biopsies (4 to 5 mm) were obtained from bilateral popliteal fossae. These samples were defined as the unwounded skin (baseline), with the Vaseline and Neosporin groups on the left and right, respectively. After punching, the bilateral popliteal fossa was started with daily medication, one side was treated with Vaseline and the other with Neosporin until healed. Patients 1 to 3 used Neosporin on the left side and Vaseline on the right side, and patients 4 to 6 used Vaseline on the left side and Neosporin on the right side to rule out the influence of the left and right sides.

Volunteers were instructed to use bandages to protect wounds, change dressings, and apply medications daily until healed. The sites were then rebiopsied on D15, and these samples were defined as wounded skin (WD15). Eight skin samples from four volunteers were collected for spatial metabolome mass spectrometry on D15 (age range: 19 to 45 years old; three females and one male; two Caucasian and two Asian). The

wounded and unwounded skins of these volunteers were collected and treated as described above.

1.2.3 Human and mouse skin microbiome collection

Six healthy adults with an average age of 28 were included in the skin microbiology study. Wang et al., 2021. Volunteers with skin diseases, infectious diseases, pregnancy, topical antibiotic treatment within 7 days, or systemic antibiotic treatment within 6 months were excluded. All volunteers signed an informed consent form. Participants were asked to refrain from washing for 24 hours before the sample collection, and no antibacterial products were used during the study. The skin microbes were collected from the popliteal fossa on the biopsy day (WD0) and the rebiopsy day (WD15). As mentioned above, the volunteers used Vaseline on one side and Neosporin on the other side every day from WD0 to WD15. A sterile cotton swab (Puritan, 25-1506 1PF TT) premoistened with lysis buffer containing 20 mM tris (pH 8.0; Quality Biological, 723017), 2 mM EDTA (Sigma-Aldrich, E4884), and 1.2% Triton X-100 (Sigma-Aldrich, T9284) was rubbed 40 times at the microbial collection site, covering 6 cm^2. Following the same preparation steps, another swab was waved in the air as a blank control. For mouse skin microbiome collection, we first shaved the back hair with hair clippers. On WD5, we rubbed the skin around the wound 40 times with the swab premoistened in the lysis buffer as described above to collect wound bed microbiome.

1.2.4 WIHN model

All animal experiments were carried out according to our previous WIHN model protocol. Wang et al., 2021; Nelson et al., 2015. In short, 21-day-old male and female mice weighing 8 to 12 g with hairs in the first telogen stage were selected. Mice were anesthetized with isoflurane, shaved, and denuded of 1.44 cm^2 full-thickness skin on the lower center of the back, using sterile procedures. The operation day was defined as WD0, and the treatment was performed at WD3 according to each experimental design. At about WD14, the wound scab would fall off. We defined it as scab-detached day (SD0), which is the time point when hair regeneration began. On day 24 after the procedure (WD24), the number of regenerated hair follicles is measured. We visualized the regenerated hair follicles and quantified them using confocal scanning laser microscopy (CLSM), as described before. Nelson et al., 2015. In GF mice, we performed the procedure in the bubble of the GF laboratory of the Johns Hopkins School of Public Health. In SPF mice, we performed the procedure in a biological safety hood in the Johns Hopkins School of Medicine. *S. aureus* (1×10^7/50 μL) was injected under the scab on

WD3. We also injected 20 μL of 100 nM LW6 (Selleck Chemicals), 1 mM glutamine (Gibco), 200 nM CB839 (Cayman Chemical), 500 nM FX11 (Sigma-Aldrich), or 200 nM UK5099 (Cayman Chemical) under the scab every other day from WD3 to SD0.

1.2.5 Human and mouse keratinocyte isolation, culture, and treatment

Human keratinocytes were obtained from discarded foreskins of male newborns, as described previously. Wang et al., 2021. After the foreskin was cut and laid flat, it was placed in 0.4% sterile dispase II (Sigma-Aldrich, D4693) overnight at 4°C. The next day, sterile forceps were used to separate the epidermis and dermis. The epidermis was subsequently sectioned and digested in trypsin-EDTA (Lonza, CC-5012) for 15 min at 37°C. Trypsin Neutralizing Solution (TNS) (Lonza, CC-5002) was used to terminate the digestion. After filtering the cells through a 6-μm filter and centrifuging them at 2000 rpm for 5 min, cells resuspended the keratinocytes in Keratinocyte Growth Medium (KGM) (Lonza, 00192152) and placed them in a humidified, 37°C incubator with 5% CO_2. The medium was changed every other day. Mouse keratinocytes were obtained from male and female newborn mice. After euthanizing six newborn mice and sterilizing them in 75% ethanol, we collected the skin and placed it in 0.4% sterile dispase II (Sigma-Aldrich, D4693) overnight at 4°C. The next day, sterile forceps were used to separate the epidermis from the dermis. Cells were collected as described above for human keratinocytes. All primary keratinocytes were passaged for at least two generations to remove contaminating cells/impurities. Mouse and human keratinocytes were cultured in KGM (Lonza, 00192152) or glutamine-deficient Dulbecco's modified Eagle's medium (Lonza, BE12-614F) and treated with 1×10^7 /mL *S. aureus*, 1 mM glutamine (Gibco), 20 nM CB839 (Cayman Chemical), 50 nM FX11 (Sigma-Aldrich), 20 nM UK5099 (Cayman Chemical), or rmIL-1β (100 ng/mL; R&D Systems) according to the design of the different experiments. For the siRNA transfection, transfected keratinocytes in 12-well plates with 10 nM Hlif-1α siRNA or Slc1a7 siRNA (Santa Cruz Biotechnology)– specific or scrambled sequences (Santa Cruz Biotechnology) for 48 hours using Lipofectamine RNA iMAX (Thermo Fisher Scientific). For hypoxia experiments, keratinocytes were cultured in a 2% O_2 incubator at 37°C for 48 hours.

1.2.6 Bacteria strains and preparation

S. aureus (NRS384) was streaked onto trichostatin A (TSA) with a sterile loop. After overnight culture at 37°C, single fluorescent colonies were selected from the plate, inoculated into TSB (BD Bacto, 8330706), and then shaken at 37°C for 18 hours. The bacterial culture was diluted 50-fold with TSB and incubated for another 3 hours to reach

the exponential growth period. The bacterial suspension was centrifuged, washed, and resuspended in sterile PBS according to the concentration required for the experiment. Bacteria at the final concentration were plated on TSA or LB and cultured overnight. The number of colony-forming units was determined by absorbance (A600).

1.2.7 Histology, immunofluorescence, and fluorescence microscopy

After obtaining human and mouse skin samples, the samples were flattened and quickly placed them into 4% paraformaldehyde (PFA; Thermo Fisher Scientific, J19943-K2). After 48 hours of fixation, biopsies were submitted to the Johns Hopkins University Oncology Tissue Service Core. The biopsies were embedded in paraffin and then sliced into 4-μm thick sections. The biopsy sections were mounted on glass slides and stained with hematoxylin and eosin (H&E). Biopsy sections were deparaffinized and then used for antigen retrieval with Target Retrieval Solution. After washing and permeabilizing the sections in TBST [tris-buffered saline (Quality Biological, 351-086-101) containing 0.1% Tween 20 (Sigma-Aldrich, P2287)], biopsy sections were incubated for 1 hour at room temperature in blocking buffer composed of 5% goat serum and 1% bovine serum albumin (Fisher Bioreagents, BP9703-100). The sections were then incubated overnight at 4°C with the primary antibody dissolved in antibody diluent (Agilent Dako, S0809). The primary antibodies used are as follows: Krt15 (Sigma-Aldrich, HPA023910), active β-catenin (Sigma-Aldrich, 05-665), Il-1β (Abcam, Ab2105), Krt1(Abcam, AB185628), Krt17 (Abcam, ab53707), Cox-2 (Thermo Fisher Scientific, PA5-17614), Col17a1 (Abcam, ab184996), and Ube2c (Abcam, ab252940). After the sections were washed with TBST, they were then incubated with fluorescently bound secondary antibody: Alexa Fluor 488 anti-mouse immunoglobulin G (IgG; Invitrogen, A-11001), Alexa Fluor 488 anti-rabbit IgG (Invitrogen, A-11008), and Alexa Fluor 594 anti-rabbit IgG (Invitrogen, A-11037) corresponding to the primary antibody strain for 1 hour at room temperature. Last, after the final TBST washing, cell nuclei were stained with 4′,6-diamidino-2-phenylindole. All slides were imaged using DFC365FX (Leica), and the fluorescence intensity was quantified with ImageJ. For keratinocyte staining, cells were cultured on sterile cover slides and grown in the incubator until 70% confluent. Cells were then fixed in 4% PFA for 20 min at room temperature, washed with PBS, and incubated in 0.1% Triton X-100 for 15 min at room temperature. Keratinocyte blocking, primary antibody and secondary antibody incubation, and fluorescence intensity quantification were carried out as described above for tissue.

1.2.8 RNA isolation and quantitative real-time PCR

Total RNA was isolated from homogenized, freshly collected human and mouse skin and from human and mouse keratinocytes using the RNeasy Mini Kit (Qiagen). The concentration and purity of RNA were determined by microspectrophotometry (NanoDrop2000c, Thermo Fisher Scientific). RNA was reverse-transcribed into complementary DNA with a kit (Applied Biosystems), and the relative expression of the gene of interest was detected by TaqMan probes with FAM dye from Applied Biosystems including murine Krt15 primers (Mm00492972_m1), murine Wnt7b primers (Mm01301717_m1), murine Krt1 primers (Mm00492992_g1), murine Krt7 primers (Mm00468876_m1), murine Hif-1α primers (Mm00468869_m1), murine Shh primers (Mm00436528_m1), murine Il-1β primers (Mm00434228_m1), human KRT1 primers (Hs00196158_m1), and human KRT15 primers (Hs00856927_g1). Expression levels were compared to those of constitutive genes murine Rplp0 (Mm00725448_s1), human RPLP0 (Hs00420895_gH), and murine β-actin (Mm02619580_g1), which were detected by TaqMan probes with VIC dye.

1.2.9 16S rRNA gene extraction, PCR amplification, and sequencing

For 16S rRNA gene sequencing, human skin microbial samples were sent to CosmoID in Maryland, and mouse skin microbial samples were sent to University of Michigan Medical School, Microbial Systems Molecular Biology Laboratory. Details of 16S rRNA gene extraction, PCR amplification, and sequencing have been reported previously. Wang et al., 2021.

1.2.10 Enzyme-linked immunosorbent assay

For each sample, we extracted 20 μg of protein from 1×10^6 keratinocytes after 72 hours of treatment. We also extracted 20 μg of protein from the wound bed of each mouse at WD5. Commercial assay kits were used to quantify the expression of glutamate (Abcam, ab83389) and IL-1β (Abcam, ab197742) in cells and tissues.

1.2.11 Mass spectrometry

Mouse and human skin samples were quickly frozen in liquid nitrogen, embedded in unflavored gelatin (Oak Brook, NY), and frozen overnight at −80°C. The next day, a cryostat was used to slice the tissue block into 15-μm sections. The skin sections were adhered to glass slides with an indium tin oxide layer. HTX Imaging M5 TM-Sprayer was used to apply α-cyano-4-hydroxycinnamic acid (CHCA; 10 mg/mL) matrix to the skin slices. Slices were sprayed six times from top to bottom at 80°C. The spraying capacity of the nozzle was 100 mL/min, and the nozzle was moved at 100 cm/min. 2-mm spacing was used, a spraying pressure of 10 psi, and an air velocity of

3000 mL/min. The distance between the nozzle and the tissue was 4 cm, and the drying time was 20 s. The processed tissue was placed in a vacuum desiccator until being used for MSI analysis.

1.2.12 MALDI MSI

The 15T Solarix FT-ICR (Bruker Daltonics, Billerica, MA) was set to positive ion mode, and the detection mass range was 100 to 800 mass/charge ratio. The laser spot was set to 10 μm and the grating distance to 25 μm. Each pixel was irradiated with 800 continuous lasers, and the matrix α-cyano-4-hydroxycinnamic acid(CHCA), 2,5-dihydroxybenzoic acid (DHB), and lipid standard mixture were used for external calibration on the stainless steel matrix-assisted laser desorption/ionization (MALDI) target. FtmsControl, FlexImaging, and SCiLS Lab were used for image processing. The spectra was normalized for all compounds to count the total ions to reduce the effect of matrix hot spots. Then, MSIreader was used for visualization and relative quantification of the slices. The control group and the treatment group were processed on the same day.

1.2.13 Microarray and bioinformatic analysis

RNA was submitted from the skin of GF mice, SPF mice, *S. aureus*– treated mice, PBS-treated mice, and human popliteal fossae to the Johns Hopkins Deep Sequence Center. The RNA was sequenced by human and murine 1.0ST exon sequencing according to the manufacturer's standard protocol. The original Affymetrix CEL data were standardized using Robust Multichip Analysis (RMA) algorithm for comparison. The data were uploaded to the Gene Expression Omnibus (GEO) under accession numbers GSE158613, GSE158614, and GSE158616.

To calculate the metabolism score, genes of interest were identified in each metabolism pathway from the Kyoto Encyclopedia of Genes and Genomes (KEGG), GSEA-Hallmark, or GO databases and then used the RMA normalization method to convert gene expression of each identified gene to a z-score to obtain the relative expression of the two groups of samples as previously described. Wang et al., 2020. The principal components analysis (PCA) algorithm assigns different weighted coefficients according to the contribution of different genes in the metabolism pathway and finally yields the metabolism score by adding the z-score of each single gene in the pathway with its paired coefficient. For the analytic code and introduction of the algorithm, please refer to the GitHub IOBR package (version 0.99.9, date of access 17 June 2021). Zeng et al., 2021. Briefly, PCA used the following method to calculate the metabolism score of each sample:

$$\text{Metabolism score} = \sum PC1i - \sum PC1_j$$

In this equation, *i* is the *z*-score of the gene whose Cox coefficient is positive, and *j* is the *z*-score of the gene whose Cox coefficient is negative. The GSEA analysis was carried out on the GSEA website. The relevant biological processes and genes were obtained from KEGG, GSEA, GO, and published literature.

1.2.14 scRNA-seq and bioinformatic analysis

R program was used for scRNA-seq analysis. Self-test dataset GSE190175 were generated and used external WIHN dataset GSE108677. For our in-house mouse data, we obtained two samples (wound center and wound periphery) by pooling tissue from five WT mice for a total 12,760 total cells. The scars of mice were used at SD0 and defined the site of hair follicle regeneration in the center of the wound as the wound center, and the site of non-regenerated hair follicles in wound periphery was defined as the wound periphery. Tissues were digested into single cells and send to Johns Hopkins Medical Institute (JHMI) Deep Sequencing and Microarray Core to preform 10× single-cell transcriptome sequencing. Samples were analyzed from the wound center and wound periphery separately. Seurat package (version 4.0.5) was used to obtain the gene expression matrix for standardized analysis. The t-Distributed Stochastic Neighbor Embedding (t-SNE) function was used to cluster the single cells into five groups based on DEGs according to known specific markers: keratinocytes, fibroblasts, immune cells, endothelial cells, and pericytes. Then, the keratinocytes were clustered into seven subtypes according to published keratinocyte markers: basal1, basal2, basal3, proliferative, spinous, HG, and unknown. Haensel et al., 2020. The interactions between different cell types or keratinocyte subtypes were analyzed with R package Cellchat (version 1.1.3). Jin et al., 2021. Signature genes used to generate the scores were derived from KEGG or gene set variation analysis (GSVA). Hypoxia, metabolism, IL-1 signaling, and keratinocyte differentiation scores were calculated using the PCA method as described above. GO enrichment analysis was carried out with R package Clusterprofiler (version 3.11.1). The pseudotime analysis was carried out with the R package Monocle (version 2.22.0). During the process of WIHN, keratinocytes undergo a transition from one state to another, expressing different sets of genes in different states. The dynamic changes of this expression are transcriptionally regulated, that is, some genes are activated and others are silenced. Monocle learns the dynamics of this gene through a reverse embedding graph algorithm and builds trajectories. For GSE108677, there are two female mice wound bed tissue pooled in each group, four

groups including SWD8, SWD14, large wound day 14 center (LWD14-center), and LWD14-periphery, for a total of eight mice and 15,710 cells. nFeature_RNA > 200 and nCount_RNA > 1000 and percent.mt < 20 were used to screen out high-quality cells and remove exogenous RNA, transfer RNA, and mitochondrial RNA. The Seurat package were used to obtain the gene expression matrix for standardized analysis. Then, t-SNE function was used to group the single cells into 14 clusters based on DEGs. These 14 clusters were divided into six groups according to the specific cell markers: keratinocytes, endothelial cells, fibroblasts, pericytes, immune cells, and a small number of unknown cells. Hypoxia, metabolism, and IL-1 scores were calculated using the PCA method as described above. Signature genes were used to generate the scores were derived from KEGG or GSVA. GO enrichment analysis was performed using R package Clusterprofiler.

The R package Monocle was used for pseudotime analysis. The interactions of different cell types were analyzed using R package Cellchat. To identify DEGs, keratinocytes were separated into two groups: wound center and wound periphery. R package was used limma to define DEGs among these two groups. To estimate gene expression changes, an empirical Bayesian approach was utilized using moderated t tests. Significance criteria (adjusted P value < 0.05) were used to determine the DEGs among High and Low Glu scores as determined by R package limma. Benjamini-Hochberg correction for multiple testing was used to calculate the adjusted P value. DEGs among keratinocytes from the wound center and periphery were defined using the same method.

1.2.15 Proteomic analysis

Briefly, mouse SD0 scars were collected, divided into wound center and wound periphery, with three mice in each group. A commercial protocol was used to extract skin proteins, as well as a Waters nanoACQUITY UPLC system and an Orbitrap Fusion Tribrid mass spectrometer for proteomic measurement. The specific processing procedures can be referred to in previous research. Kim et al., 2019. For proteomic analysis, PCA algorithm as described above, generated metabolism scores based on the expression of metabolic signature genes. Metabolic signature genes were obtained from KEGG, Hallmark, and the published literature.

1.2.16 16S rRNA gene sequence bioinformatic analysis

Briefly, collected skin microbiome were sent to CosmoID in Maryland and University of Michigan Medical School, Microbial Systems Molecular Biology Laboratory for 16S rRNA sequencing. Fastx_toolkit_v0.0.14 was used for the raw 16S

rRNA gene sequencing data analysis, as shown previously. Wang et al., 2021. Based Taxonomic Classification Method (BLCA) and GreenGenes were used for taxonomic classification. QIIME2 was used for operational taxonomic unit analysis and Shannon diversity. α- and β-Diversity was calculated by q2-diversity plugin. The PCA of β-diversity was generated via R package stats cmdscale. Microbiome data were visualized by R package ggplot2.

1.2.17 Statistical analysis

All *in vivo* and *in vitro* representative data were from at least three individual substances and two to three independent experiments. Scatterplots and bar graphs are presented as means ± SE. The box plot indicates the minimum, first quartile, median, third quartile, and maximum values. Comparisons between two groups were analyzed by unpaired Student's t test. For multiple-group comparisons, we used one-way analysis of variance (ANOVA) as a parametric method. Statistical significance was defined by P value (*P < 0.05, **P < 0.01, ***P < 0.001, and ****P < 0.0001), and the P values were two-sided. P values less than 0.05 were considered statistically significant. NS indicates no significant difference.

Correlation coefficients were computed by distance correlation and Spearman analyses. To identify significant DEGs, the Benjamini-Hochberg method was applied to convert the P values to false discovery rates. All statistical analyses were carried out with R.

1.3 Results

1.3.1 Bacteria stimulate WIHN through keratinocyte-dependent IL-1β–MyD88

In a previous study, six skin microbial gradient models were used to show that skin microbes promote WIHN. By screening five top mouse skin commensal microbes, it was found that *S. aureus* had the strongest ability to promote WIHN; therefore, *S. aureus* was used as a representative of commensal microbes to further research mechanism. Wang et al., 2021. Bacterial load correlates in a dose-responsive manner to WIHN. Compared to standard laboratory specific pathogen–free (SPF) mice, germ-free (GF) mice have lower WIHN (fold change = –21.7, $P = 5.8 \times 10^{-8}$), while SPF mice treated with *S. aureus* have higher WIHN (fold change = 3.5, $P = 2.1 \times 10^{-7}$) (FIG. 8A). Taxonomy analysis verified that the relative abundance of bacteria in the wound beds of GF, SPF, and *S. aureus*–treated mice increased, respectively, and significantly (FIG. 8C). Unlike in SPF control mice, Staphylococcus was the most common bacterial strain in *S. aureus*–treated mice, with the percentages of other bacteria mostly lower than in SPF

mice, showing that exogenous *S. aureus* suppresses other bacteria (FIG. 8D). Wang et al., 2021. In *S. aureus*–treated wounds, β-catenin and Krt15—markers of hair follicle regeneration and HFSCs, respectively—were markedly increased at scab detachment day 0 (SD0), the time when hair follicle regeneration begins (FIG. 8B). It also confirmed that Il-1β–/– mice regenerate poorly (fold change = –42.6, $P = 2.1 \times 10^{-7}$), and this could not be rescued by *S. aureus* treatment (FIG. 8, FIG. 8G and FIG. 8H). Last, previous findings were validated and that K14-Myd88–/– mice exhibit significantly lower regeneration than wild-type (WT) mice (fold change = –3.9, $P = 1.0 \times 10^{-4}$) and are likewise unresponsive to *S. aureus* rescue (FIG. 8, FIG. 8I and FIG. 8J). Taxonomy analysis showed that the relative abundance of bacteria in the wound bed of K14-Myd88–/– and Il-1β–/– mice was significantly lower than that in WT mice, suggesting an interesting host-commensal cross-talk (FIG. 8E). *Staphylococcus* was significantly higher in the WT mouse wound bed, whereas *Pseudomonas* was the dominant bacteria in the wound beds of K14-Myd88–/– and Il-1β–/– mice (FIG. 8F). Together, these results confirm that the skin microbiome induces WIHN through keratinocyte-dependent IL-1β–Myd88 signals.

1.3.2 Bacteria induce keratinocyte IL-1β production via glutamine metabolism

The next goal was to understand how bacteria induce IL-1β to promote regeneration. A previous study showed that different types of bacteria promote hair follicle regeneration in a Toll-like receptor 2/3 (TLR2/3)–independent mechanism, indicating that bacteria might promote regeneration through nonspecific pathways rather than through pattern recognition receptors. One possibility is that the microbiome may regulate metabolism in the microenvironment to promote IL-1β signaling. Roux et al., 2021; Chen et al., 2021. To explore this, the energy metabolism of fatty acids, glucose, glycan, pyruvate, glutamine, and glutamate using were examined transcriptome Gene Ontology (GO) to calculate different metabolic scores in the wounds of mice with different microbial loads (FIG. 1A). The most significantly up-regulated metabolic pathway was glutamine metabolism, which increased with bacterial load. Notably, the increase in glutamine metabolism correlated with regenerative capacity in SPF (high WIHN) mice versus GF (low WIHN) and *S. aureus* (high WIHN) versus phosphate-buffered saline (PBS) (low WIHN) mice (FIG. 1A). Because a recent study has shown that glutamine metabolism activates HFSCs and promotes the anagen phase in hair follicles, glutamine and glutamate metabolic gene expression was compared in the two above contexts, plus a third from a published literature: low (C57Bl/6J) versus high

(B6/FVB/SJL) WIHN in untreated WT mice (different mouse strains). Kim et al., 2020; Nelson et al., 2015. Most of the glutamine and glutamate genes, especially glutaminase (Gls), were more highly expressed in high WIHN mice and positively correlated with the skin bacterial load (FIG. 1B). The expression levels of Gls and Gls2 were elevated in the high WIHN group (FIG. 1C). Gene set enrichment analysis (GSEA) also confirmed that glutamine and glutamate metabolism were highly expressed in the wounded skin of mice with high bacterial loads and high regeneration (FIG. 1, FIG. 1D and FIG. 1E).

Using mass spectrometry imaging (MSI) of the spatial metabolome to visualize the expression of different metabolites, it was found that the trace amines, cholesterol, and triacylglycerol did not increase significantly compared to their levels in unwounded skin (baseline), during wounding [wound day 5 (WD5)] or at the beginning of hair regeneration (SD0; FIG. 9A to FIG. 9C). On the basis of the previous studies, metabolites were measured that promote hair follicle growth, including gallic acid, α-ketoglutarate, inosine, inosine monophosphate, spermidine, and spermine. Boisvert et al., 2017; Chai et al., 2019; Allmeroth et al., 2019; Park et al., 2020. Likewise, it was found that these metabolites did not exhibit a significantly consistent trend with the bacterial load of the skin at any tested time point (FIG. 10A to FIG. 10F). Both glutamine and glutamate levels, however, were greater in mice with high bacterial load and high WIHN during WD5 and SD0 (FIG. 1F and FIG. 8K and FIG. 11A). There was no significant difference, however, in glutamine and glutamate levels between high and low bacterial loads in the baseline (FIG. 12A and FIG. 12B). These data show that bacteria induce glutamine metabolism in keratinocytes during wounding. To confirm, mouse wound proteins also were collected at the start of hair follicle regeneration and detected by enzyme-linked immunosorbent assay (ELISA) that glutamate was highly expressed in high-WIHN mice (FIG. 2A). To determine whether glutamine metabolism affects IL-1β expression in keratinocytes, thereby promoting regeneration, mouse keratinocytes were isolated, cultured, and treated with glutamine. It was found that glutamine promoted Il-1β mRNA expression in keratinocytes (FIG. 2B). Keratinocytes treated with the glutaminase inhibitor CB839 had decreased Il-1β expression (FIG. 2B), an effect that could be rescued by adding exogenous glutamine (FIG. 2B). Then, to test the role of *S. aureus in vitro* it was found that keratinocytes treated with *S. aureus* induced Il-1β mRNA expression (FIG. 2B). Notably, CB839 significantly inhibited *S. aureus* induced Il-1β expression (FIG. 2B), suggesting that induction is mediated by glutamine metabolism. In contrast, other metabolites had no effect on keratinocyte IL-1β

production. Keratinocytes treated with lactase dehydrogenase inhibitor (FX11) or glucose oxidation inhibitor (UK5099) did not have significantly decreased Il-1β levels compared to vehicle-treated controls (FIG. 2C). CB839, however, inhibited mouse keratinocyte Il-1β protein expression and release (FIG. 2C). CB839 also inhibited the production of Il-1β protein induced by *S. aureus* and *S. aureus* supernatants, confirming the mRNA results (FIG. 2C). Last, investigated was the *in vivo* effect of glutamine metabolism on the production of IL-1β. *S. aureus* induced and CB839 inhibited both Il-1β protein and mRNA production (FIG. 2D). In human keratinocytes, CB839 also inhibited IL-1β production (FIG. 2E). These results showed that skin bacteria, specifically *S. aureus*, promote keratinocyte glutamine metabolism and that glutamine metabolism is essential for the production of keratinocyte IL-1β.

Last, we tested the effect of bacteria on human wound metabolism in a small trial of healthy adult volunteers by performing bilateral punch biopsy wounds of the skin at the popliteal fossae (behind the knees) and subsequent treatment with a vehicle (Vaseline petroleum jelly) or a topical antibiotic (Neosporin). A second biopsy was performed to collect healing tissue. In an analysis of the transcriptome, it was found that wounding of skin induces large shifts in metabolic patterns and that glutamine metabolism was highly induced in wounded skin (FIG. 2F). This finding is consistent with previous studies showing that glutamine metabolism increases during damage response. Biolo et al., 1997; Kesici et al., 2015. Previous research also showed that using antibiotic ointment significantly reduced wound healing speed and altered the microbiome in both mice and humans. Wang et al., 2021; Archer et al., 2019. Glutamine metabolism, glutamate metabolism, and bacterial relative abundance did not differ between the left and right sides on human unwounded skin (FIG. 12C and FIG. 12D). After wounding, however, the total amount of bacteria on the side treated with Neosporin was significantly lower than that on the side treated with Vaseline (FIG. 12D). The Vaseline-treated side was characterized by a significant increase in the dominant bacteria, *Staphylococcus*, in the popliteal fossa (FIG. 12E). In both unwounded and wounded skin, *S. aureus* and *Staphylococcus epidermidis* were the dominant Staphylococcus species (FIG. 12F). Consistent with these results, antibiotic treatment significantly reduced glutamine *metabolism* genes in the human wound bed (FIG. 2F). Furthermore, MSI showed that glutamine and glutamate levels decreased in the antibiotic-treated human wound bed (FIG. 2, FIG. 2G and FIG. 2H, and FIG. 11B). These data indicate that commensal

bacteria on human skin can also induce glutamine metabolism and improve regeneration, which is consistent with our *in vitro* results. Wang et al., 2021.

1.3.3 Glutamine metabolism induces the expression of stem cell markers and regenerative signaling in vitro

Next, the effects of glutamine metabolism were investigated on keratinocyte regeneration signals *in vitro*. Wang et al., 2021; Nelson et al., 2015; Kim et al., 2019. It was found that CB839 inhibited the regeneration signals Wnt7b and Shh and the stem cell marker Krt15 and induced the terminal differentiation marker Krt1 in keratinocytes (FIG. 3A). CB839, however, did not inhibit Wnt7b and Krt15 in keratinocytes from Myd88–/– and Il-1β–/– mice (FIG. 3B). Thus, glutamine induces regeneration associated genes through IL-1β–MyD88 signaling. CB839 inhibits the protein expression of active β-catenin and KRT15 in human keratinocytes but induces the protein expression of KRT1 (FIG. 3C). Notably, the addition of mouse recombinant Il-1β (rmIl-1β) can rescue the inhibition of Wnt7b and Shh and the promotion of Krt1 by CB839 in mouse keratinocytes (FIG. 3D). These data suggest that IL-1β is a downstream signal of glutamine-induced regenerative gene expression.

1.3.4 Glutamate is required for baseline and bacteria-induced WIHN

The effect of glutamine metabolism on hair follicle regeneration *in vivo* was studied The addition of exogenous glutamine to healing wounds induced WIHN (fold change = 2.2, $P = 2.8 \times 10^{-4}$), whereas CB839 inhibited WIHN (fold change = –3.2, $P = 5.4 \times 10^{-4}$) (FIG. 4A). Consistent with this effect, glutamine-induced glutamate production at SD0, whereas CB839 inhibited it (FIG. 4B). To determine whether other metabolic pathways could affect WIHN, separate cellular respiration pathways were blocked (FIG. 12G). Because previous studies have shown that lactate metabolism is essential for activating HFSCs, FX11 was used to inhibit lactase dehydrogenase. Flores et al., 2017. Although FX11 inhibited baseline WIHN (fold change = –2.3, $P = 1.2 \times 10^{-4}$), it did not inhibit *S. aureus*–induced WIHN (P = 0.30) (FIG. 4C). Hence, lactate metabolism promotes hair follicle regeneration but does not play a key role in the regeneration induced by bacteria. To confirm that the effect of CB839 on WIHN is not simply a result of metabolic deficiencies, citric acid cycle metabolism were also reduced by preventing pyruvate entry with the inhibitor UK5099 (FIG. 12G). UK5099, however, did not inhibit hair follicle regeneration (P = 0.31) (FIG. 4D). In contrast, CB839 inhibited *S. aureus*–induced WIHN (fold change = –2.3, $P = 4.9 \times 10^{-4}$; FIG. 4E). It also inhibited baseline and *S. aureus*–induced glutamate and Il-1β expression at SD0 (FIG.

4F). This finding is consistent with *in vitro* data, which showed that glutamate expression decreases when mouse keratinocytes are cultured in glutamine-deficient medium (FIG. 12H). Similarly, in the absence of glutamine, bacterially induced glutamate expression in keratinocytes also decreased (FIG. 12H). Collectively, these results indicate that hair follicle regeneration induced by bacteria depends on glutamine metabolism. Last, to confirm that the promotion of WIHN by glutamine metabolism is keratinocyte dependent, we used keratinocyte Myd88 and myeloid Myd88 knockout mice to exclude the role of myeloid Myd88. WT were treated, Il-1β–/–, K14-Myd88–/–, and LysM-Myd88–/– mice with glutamine. Glutamine induced WIHN only in WT and LysM-Myd88–/– mice (fold change = 2.5, $P = 3.4 \times 10^{-4}$), indicating that glutamine metabolism promotes hair follicle regeneration through IL-1β–keratinocyte–dependent Myd88 signaling in keratinocytes (FIG. 4G).

1.3.5 S. aureus stimulates glutamine metabolism, IL-1β production, and WIHN through hypoxia-induced HIF-1α signaling

Previous studies have shown that increased bacterial loads, especially of *S. aureus*, can induce hypoxia in the skin. Separately, studies have shown that hypoxia-induced HIF-1α signaling promotes glutamine metabolism and IL-1β synthesis. Wickersham et al., 2017; Stegen et al., 2016; Sun et al., 2014. A goal of this Example was to determine the mechanism by which bacteria promote glutamine metabolism to induce IL-1β production using GSEA to detect the state of hypoxia in human and mouse wounds under different bacterial loads. The three human and mouse studies were reexamined correlating bacterial load to regeneration and a fourth comparison of high versus low WIHN among different mouse strains. In all cases, regenerative capacity was correlated with a hypoxic transcriptomic signature (FIG. 5A). Most hypoxia-related genes are highly expressed in wounds with high regeneration. Hif-1α mRNA was especially high, as confirmed by quantitative polymerase chain reaction (PCR) (FIG. 5, FIG. 5B and FIG. 5C). The changes were examined in keratinocyte glutamine metabolism and Il-1β under hypoxic conditions *in vitro*. CB839 inhibited the expression of Il-1β under 2% oxygen (FIG. 5D), as it had under normal oxygen conditions (FIG. 2B). Subsequently, the effects of Hif-1α was compared on glutamine metabolism and Il-1β expression in cultured mouse keratinocytes *in vitro* under normal oxygen (20%) and hypoxic conditions (2% oxygen). Under normoxia, knockdown of Hif-1α with Hif-1α small interfering RNA (siRNA) (FIG. 12I) reduced Il-1β production, but addition of exogenous glutamine partially reversed this effect, suggesting that glutamate mediates

Hif-1α induction of Il-1β production (FIG. 5E). It was found that the hypoxic environment induced keratinocyte glutamine metabolism, Il-1β expression, and expression of proregenerative Wnt7b when compared to levels in normoxic cells (FIG. 5, FIG. 5F and FIG. 5G). By knocking down Hif-1α, Il-1β expression was inhibited of keratinocytes cultured under hypoxic conditions (FIG. 5G). These results show that hypoxia induces glutamine metabolism through HIF-1α signaling, which then induces IL-1β production and regeneration signals (FIG. 5, FIG. 5E to FIG. 5G). Bioinformatic analyses revealed that SLC1A7, a glutamate transporter, is highly expressed in mouse and human skin with high bacterial loads and high WIHN (FIG. 1B and FIG. 2F). A previous study showed that glutamate transporter expression is mediated by HIF-1α signaling. Kanai et al., 2013. Therefore, the expression of Slc1a7 in the keratinocytes were knockdown. Although knocking down Slc1a7 reduced glutamate expression in keratinocytes, glutamate expression induced by *S. aureus* did not decrease significantly (FIG. 12J).

Thus, other glutamine transporters might play a compensatory role when glutamate expression is stimulated by *S. aureus*. Furthermore, silencing of Hif-1α also significantly reduced *S. aureus*–induced glutamine metabolism and the expression of Il-1β, regeneration signal Wnt7b, and stem cell marker Krt7 (FIG. 5H). *In vivo*, confirmed findings by injecting the HIF-1α inhibitor LW6 into mouse wounds and evaluating WIHN. It was observed that LW6 inhibited both baseline WIHN (fold change = −5.1, P = 2.0×10^{-5}) and *S. aureus*–induced WIHN (fold change = −4.1, P = 2.8×10^{-6}) (FIG. 5I). Likewise, LW6 inhibited the expression of glutamate and Il-1β in the wound at the beginning of hair follicle regeneration (FIG. 5J). These results indicate that hypoxia-induced HIF-1α signal stimulates glutamine metabolism and IL-1β production in keratinocytes *in vitro* and *in vivo*, inducing proregenerative signals and thereby promoting WIHN.

1.3.6 Hypoxia and glutamine metabolism in keratinocytes during WIHN

It was found that bacteria promote keratinocyte hypoxia and glutamine metabolism *in vivo* and *in vitro*, which, in turn, induce regeneration in mice and humans. It was verified our finding in public single-cell RNA sequencing (scRNA-seq) databases for four conditions: normal skin, small wound, large wound center (WIHN), and large wound periphery (non-WIHN) under GSE108677. Abbasi et al., 2020. Five cell types have been defined according to known markers, including keratinocytes, fibroblasts, immune cells, endothelial cells, and peripheral cells (FIG. 13A). Haensel et al., 2020.

Previous studies have shown that γδT cells in the wound bed release Fgf9 to activate the Wnt signal of dermal fibroblast, which is necessary to initiate hair follicle regeneration. Afterward, during reepithelialization (SD0), epidermal keratinocytes coalesce to the hair germ (HG) and release Wnt ligands to activate dermal papilla. Gay et al., 2013; Ito et al., 2007. These extracellular signals promote embryonic-like hair follicle morphogenesis. Given such examples of the importance of communications between immune cells, fibroblasts, and keratinocytes in WIHN, it was investigated the different interactions between keratinocytes and other cells in the microenvironment of WIHN (wound center) and non-WIHN (wound periphery). It was found that the intensity of intercellular communication in WIHN was greater than that of non-WIHN, especially for intercellular growth factors (FIG. 13B). The focus was on keratinocytes for in-depth exploration (FIG. 13A, black arrow). Consistent with the results of our bulk RNA-seq on mice and humans, scores for hypoxia, oxidative phosphorylation, and glutamine and glutamate metabolism were significantly higher in keratinocytes isolated from wounds than in those isolated from normal skin. These scores also were higher in the large wound centers (WIHN) than in the periphery (non-WIHN), showing that keratinocytes in the wound bed, especially in the regenerative hair follicles, required increased energy and glutamine metabolism (FIG. 13C). It was found that in keratinocytes, the hypoxia score was positively correlated with IL-1 signal ($R = 0.69$, $P < 2.2 \times 10^{-16}$) scores (FIG. 13D). By comparing the central (WIHN) and peripheral (non-WIHN) keratinocytes, it was found that the WIHN keratinocytes highly expressed protein synthesis and mitochondrial metabolism pathways, which induced HG development. In contrast, the non-WIHN keratinocytes highly expressed the extracellular matrix synthesis pathway, which is known to be elevated in scar formation (FIG. 13E). Because WIHN is a dynamic process, we used pseudotime analysis to reconstruct the development of keratinocytes (FIG. 13F). It was found that in large wounds, especially at the center (WIHN), keratinocytes were concentrated in the early developmental stage, when the stem cell potential was stronger, whereas in small wounds (non-WIHN), keratinocytes were concentrated in the late developmental stage, when the stem cell potential was weaker (FIG. 13, FIG. 13F and FIG. 13G). Through the clustering of developmental reconstruction genes, it was found that cells in the early stages of development highly expressed p53, cell cycle, glutathione metabolism, and Hif-1 signals (FIG. 13H). In addition, stem cell and developmental markers (FIG. 13I) and hypoxia-related genes (FIG. 13J) decreased with pseudotime. These data are consistent with previous studies,

which showed that hypoxia is critical to the metabolic milieu of stem cell niches. Mohyeldin et al., 2010.

1.3.7 Hypoxia and glutamine metabolism during hair follicle development in WIHN

To further investigate the changes in energy metabolism of keratinocytes during hair follicle regeneration at the single-cell resolution and to confirm the effects of hypoxia and glutamine metabolism on keratinocyte differentiation and HG development, scRNA-seq was performed. It was compared the wound center (WIHN) and wound periphery (non-WIHN) in additional mice (five mice per group). Previous studies have shown that gene transcription is altered before keratinocytes migrate to the center of the wound, suggesting that the fate of keratinocytes is determined before HG development. Ito et al., 2007; Ito et al., 2005. The wound bed tissue was collected immediately before hair follicle regeneration (SD0) for sequencing. Cells were clustered in the wound center and periphery separately and used multiple markers to define different cell clusters (FIG. 6A and FIG. 6B, and FIG. 14A to FIG. 14D). Five cell types were defined: keratinocytes, fibroblasts, immune cells, endothelial cells, and peripheral cells (FIG. 6A and FIG. 6B). Interactions were found more between different cell types in the wound center than in the periphery, especially communication between various cells and keratinocytes (FIG. 6C and FIG. 14E). To explore the specific signals that play a role in the communication between cells, signals that originated or affected various cells were listed (FIG. 6D and FIG. 14, FIG. 14F and FIG. 14G). The bone morphogenic protein (BMP) signal that acts on fibroblasts and pericytes was substantially weaker in the center of the wound than in the periphery, whereas the Wnt signal that acts on vascular endothelial cells and fibroblasts was substantially stronger in the center of the wound and weaker in the periphery. These findings support studies showing that Wnt induces hair regeneration, and BMP inhibits. Ito et al., 2007; Zhang et al., 2006. The overall IL-6 signal acting on keratinocytes was substantially stronger in the center of the wound than at the periphery (FIG. 6D, red arrow). In addition, more IL-6 signaling from each cell type acted on keratinocytes in the wound center, consistent with our previous study (FIG. 6D, left). Nelson et al., 2015. It was also shown that the IL-1 signal was absent from the wound periphery and was expressed only in the center of the wound. The specific expression pattern showed that keratinocytes release IL-1, which acts in an autocrine fashion, supporting the results described above (FIG. 6D). Wang et al., 2021.

After establishing the interactions between different types of wound cells, the interactions between keratinocytes were the focus. All genes were then used for

unsupervised clustering; the keratinocytes in the wound center clustered apart from those in the periphery, indicating that they had different gene expression patterns (FIG. 6E, top). The same pattern was observed when we used only hypoxia-related gene sets for unsupervised clustering. Keratinocytes in the wound center still clustered together, as did those in the periphery, with little overlap between the two groups (FIG. 6E, bottom). This phenomenon did not occur with other gene sets (FIG. 14H), suggesting that hypoxia gene expression signatures are a major differentiator of central versus peripheral keratinocytes. Next, the metabolic status of the keratinocytes were assessed in the center and periphery. Enrichment analysis of differentially expressed genes (DEGs) between center and peripheral keratinocytes showed that the HIF-1 signal, carbon metabolism signal, glutathione metabolism, and amino acid biosynthesis were highly expressed in the center (FIG. 6F). It was found that the keratinocytes in the center had higher hypoxia, glutamine metabolism, and IL-1 signal scores (FIG. 6G). Thus, the keratinocytes in the high-WIHN wound center appear to have a higher hypoxic status and glutamine metabolism. Proteomics was used to confirm these findings. Consistent with the scRNA-seq data and our previous study, retinoic acid metabolism, glutamate metabolism, and glutathione were higher in the wound center, whereas fatty acid metabolism and glucose metabolism were lower (FIG. 14I). Kim et al., 2019. The glutamine metabolism, hypoxia, and IL-1 signaling scores calculated from the proteomic data were higher in the wound center, whereas the keratinocyte differentiation score was lower (FIG. 14J). It also was found that the hypoxia score was positively correlated with the IL-1 signaling score ($R = 0.67$, $P < 2.2 \times 10^{-16}$) (FIG. 6H). These results verified the high glutamine metabolism, hypoxia, and IL-1 signaling in the high WIHN area at both the transcript and protein levels. Because keratinocytes in the wound center are the source of epithelial components for regenerating hair follicles, were then isolated for analysis. After, GO enrichment analysis was carried out on the DEGs associated with high and low glutamine metabolism and found that keratinocytes with high glutamine metabolism have stronger adenosine 5′-triphosphate synthesis, mRNA, and protein synthesis pathways, which are necessary for hair follicle development (FIG. 6I). Keratinocytes with low glutamine metabolism had stronger extra-cellular matrix formation, intercellular adhesion, and cellular junctions, which are necessary for the formation of scar tissue and likely inhibit WIHN (FIG. 6I). To explore the fate of different keratinocyte subtypes, the keratinocytes in the wound center were clustered and labeled them according to known markers to identify six subtypes: basal1, basal2, basal3,

proliferative, spinous, and HG (FIG. 7A and FIG. 7B). Haensel et al., 2020; Joost et al., 2016. Specifically, markers such as Krt17, Lef1, Krt79, and Sox9 were used to mark HG keratinocytes and Col17a1, Cox-2, and Ube2c to mark basal and proliferating keratinocytes (FIG. 7A to FIG. 7D). Compared with other cell types in the wound center, keratinocytes had stronger IL-1 and IL-6 signal inputs as well as stronger IL-1 signal output (FIG. 14K). Moreover, HG keratinocytes had significantly higher hypoxia, glutamine, and glutamate metabolisms and IL-1 signaling than other keratinocytes, which is consistent with previous studies (FIG. 7E). Wang et al., 2021; Kim et al., 2020. Because WIHN is a dynamic process, to clarify the different states of basal cells in the context of epidermal differentiation, the differentiation state of keratinocytes were then calculated using pseudotime analysis. The development pattern followed the direction of basal, spinous, proliferative, and HG keratinocytes (FIG. 7F and FIG. 7G). The signature genes changed from stem cell markers to mature markers as pseudotime progressed (FIG. 7H). The expression of HG markers gradually increased (FIG. 7H and FIG. 7I). The developmental stages of HG were divided into six incremental stages: A to F (FIG. 7J). As HG cells developed, the metabolism of hypoxia and glutamate showed an overall upward trend (FIG. 7K). The IL-1 signal also somewhat increased; however, glucose metabolism did not change significantly (FIG. 7K). These results suggest that increased hypoxia and glutamine metabolism can maintain the stemness of keratinocytes and promote hair follicle development (FIG. 14L).

REFERENCES

All publications, patent applications, patents, and other references mentioned in the specification are indicative of the level of those skilled in the art to which the presently disclosed subject matter pertains. All publications, patent applications, patents, and other references are herein incorporated by reference to the same extent as if each individual publication, patent application, patent, and other reference was specifically and individually indicated to be incorporated by reference. It will be understood that, although a number of patent applications, patents, and other references are referred to herein, such reference does not constitute an admission that any of these documents form part of the common general knowledge in the art.

G. Wang, E. Sweren, H. Liu, E. Wier, M. P. Alphonse, R. Chen, N. Islam, A. Li, Y. Xue, J. Chen, Y. Chen, S. Lee, Y. Wang, S. Wang, N. K. Archer, W. Andrews, M. A. Kane, E. Dare, S. K. Reddy, Z. Hu, E. A. Grice, L. S. Miller, L. A. Garza, Bacteria

induce skin regeneration via IL-1β signaling. Cell Host Microbe 29, 777–791.e6 (2021).

H. Abo, B. Chassaing, A. Harusato, M. Quiros, J. C. Brazil, V. L. Ngo, E. Viennois, D. Merlin, T. Gewirtz, A. Nusrat, T. L. Denning, Erythroid differentiation regulator-1 induced by microbiota in early life drives intestinal stem cell proliferation and regeneration. Nat. Commun. 11, 513 (2020).

H. Wu, S. Xie, J. Miao, Y. Li, Z. Wang, M. Wang, Q. Yu, Lactobacillus reuteri maintains intestinal epithelial regeneration and repairs damaged intestinal mucosa. Gut Microbes. 11, 997–1014 (2020).

Y. Liu, Y. Wang, Y. Ni, C. K. Y. Cheung, K. S. L. Lam, Y. Wang, Z. Xia, D. Ye, J. Guo, M. A. Tse, G. Panagiotou, A. Xu, Gut microbiome fermentation determines the effcacy of exercise for diabetes prevention. Cell Metab. 31, 77–91.e5 (2020).

J. He, T. Chan, X. Hong, F. Zheng, C. Zhu, L. Yin, W. Dai, D. Tang, D. Liu, Y. Dai, Microbiome and metabolome analyses reveal the disruption of lipid metabolism in systemic lupus erythematosus. Front. Immunol. 11, 1703 (2020).

H. Guo, W.-C. Chou, Y. Lai, K. Liang, J. W. Tam, W. J. Brickey, L. Chen, N. D. Montgomery, X. Li, L. M. Bohannon, A. D. Sung, N. J. Chao, J. U. Peled, A. L. C. Gomes, M. R. M. van den Brink, M. J. French, A. N. Macintyre, G. D. Sempowski, X. Tan, R. Balfour Sartor, K. Lu, J. P. Y. Ting, Multi-omics analyses of radiation survivors identify radioprotective microbes and metabolites. Science 370, eaay9097 (2020).

P. Kundu, H. U. Lee, I. Garcia-Perez, E. X. Y. Tay, H. Kim, L. E. Faylon, K. A. Martin, R. Purbojati, D. I. Drautz-Moses, S. Ghosh, J. K. Nicholson, S. Schuster, E. Holmes, S. Pettersson, Neurogenesis and prolongevity signaling in young germ-free mice transplanted with the gut microbiota of old mice. Sci. Transl. Med. 11, eaau4760 (2019).

P.-F. Roux, T. Oddos, G. Stamatas, Deciphering the role of skin surface microbiome in skin health: An integrative multiomics approach reveals three distinct metabolite-microbe clusters. J. Invest. Dermatol. 142, 469–479.e5 (2021).

D. Chen, J. He, J. Li, Q. Zou, J. Si, Y. Guo, J. Yu, C. Li, F. Wang, T. Chan, H. Shi, Microbiome and metabolome analyses reveal novel interplay between the skin microbiota and plasma metabolites in psoriasis. Front. Microbiol. 12, 643449 (2021).

Y. Cai, F. Xue, C. Quan, M. Qu, N. Liu, Y. Zhang, C. Fleming, X. Hu, H. G. Zhang, R. Weichselbaum, Y. X. Fu, D. Tieri, E. C. Rouchka, J. Zheng, J. Yan, A critical role of the IL 1β–IL-1R signaling pathway in skin inflammation and psoriasis pathogenesis. J. Invest. Dermatol. 139, 146–156 (2018).

R. M. Salgado, L. Alcántara, C. A. Mendoza-Rodríguez, M. Cerbón, C. Hidalgo-González, P. Mercadillo, L. M. Moreno, R. Alvarez-Jiménez, E. Krötzsch, Post-burn hypertrophic scars are characterized by high levels of IL-1β mRNA and protein and TNF-α type I receptors. Burns 38, 668–676 (2012).

E. Rodriguez, G. S. Ducker, L. K. Billingham, C. A. Martinez, N. Mainolfi, V. Suri, A. Friedman, M. G. Manfredi, S. E. Weinberg, J. D. Rabinowitz, N. S. Chandel, Serine metabolism supports macrophage IL-1β production. Cell Metab. 29, 1003–1011.e4 (2019).

G. M. Tannahill, A. M. Curtis, J. Adamik, E. M. Palsson-McDermott, A. F. McGettrick, G. Goel, C. Frezza, N. J. Bernard, B. Kelly, N. H. Foley, L. Zheng, A. Gardet, Z. Tong, S. S. Jany, S. C. Corr, M. Haneklaus, B. E. Caffrey, K. Pierce, S. Walmsley, F. C. Beasley, E. Cummins, V. Nizet, M. Whyte, C. T. Taylor, H. Lin, S. L. Masters, E. Gottlieb, V. P. Kelly, C. Clish, P. E. Auron, R. J. Xavier, L. A. O'Neill, Succinate is an inflammatory signal that induces IL-1β through HIF-1α. Nature 496, 238–242 (2013).

C. S. Kim, X. Ding, K. Allmeroth, L. C. Biggs, O. I. Kolenc, N. L'Hoest, C. A. Chacón-Martínez, C. Edlich-Muth, P. Giavalisco, K. P. Quinn, M. S. Denzel, S. A. Eming, S. A. Wickström, Glutamine metabolism controls stem cell fate reversibility and long-term maintenance in the hair follicle. Cell Metab. 32, 629–642.e8 (2020).

R. Williams, M. P. Philpott, T. Kealey, Metabolism of freshly isolated human hair follicles capable of hair elongation: A glutaminolytic, aerobic glycolytic tissue. J. Invest. Dermatol. 100, 834–840 (1993).

R. Raizel, J. S. M. Leite, T. M. Hypólito, A. Y. Coqueiro, P. Newsholme, V. F. Cruzat, J. Tirapegui, Determination of the anti-inflammatory and cytoprotective effects ofL-glutamine andL-alanine, or dipeptide, supplementation in rats submitted to resistance exercise. Br. J. Nutr. 116, 470–479 (2016).

Y. Shi, Z. Tu, D. Tang, H. Zhang, M. Liu, K. Wang, S. K. Calderwood, X. Xiao, The inhibition of LPS-induced production of inflammatory cytokines by HSP70 involves inactivation of the NF-κB pathway but not the MAPK pathways. Shock 26, 277–284 (2006).

H. Charles-Messance, G. Blot, A. Couturier, L. Vignaud, S. Touhami, F. Beguier, L. Siqueiros, V. Forster, N. Barmo, S. Augustin, S. Picaud, J. A. Sahel, A. Rendon, A. Grosche, R. Tadayoni, F. Sennlaub, X. Guillonneau, IL-1β induces rod degeneration through the disruption of retinal glutamate homeostasis. J. Neuroinflammation 17, 1

(2020).

M. Wickersham, S. Wachtel, T. W. F. Lung, G. Soong, R. Jacquet, A. Richardson, D. Parker, A. Prince, Metabolic stress drives keratinocyte defenses against Staphylococcus aureus infection. Cell Rep. 18, 2742–2751 (2017).

F. McGettrick, L. A. J. O'Neill, The role of HIF in immunity and inflammation. Cell Metab. 32, 524–536 (2020).

J. W. Kim, I. Tchernyshyov, G. L. Semenza, C. V. Dang, HIF-1-mediated expression of pyruvate dehydrogenase kinase: A metabolic switch required for cellular adaptation to hypoxia. Cell Metab. 3, 177–185 (2006).

E. Schipani, H. E. Ryan, S. Didrickson, T. Kobayashi, M. Knight, R. S. Johnson, Hypoxia in cartilage: HIF-1alpha is essential for chondrocyte growth arrest and survival. Genes Dev. 15, 2865–2876 (2001).

O. Genbacev, Y. Zhou, J. W. Ludlow, S. J. Fisher, Regulation of human placental development by oxygen tension. Science 277, 1669–1672 (1997).

Flores, J. Schell, A. S. Krall, D. Jelinek, M. Miranda, M. Grigorian, D. Braas, A. C. White, J. L. Zhou, N. A. Graham, T. Graeber, P. Seth, D. Evseenko, H. A. Coller, J. Rutter, H. R. Christofk, W. E. Lowry, Lactate dehydrogenase activity drives hair follicle stem cell activation. Nat. Cell Biol. 19, 1017–1026 (2017).

G. Lone, E. Atci, R. Renslow, H. Beyenal, S. Noh, B. Fransson, N. Abu-Lail, J. J. Park, D. R. Gang, D. R. Call, Staphylococcus aureus induces hypoxia and cellular damage in porcine dermal explants. Infect. Immun. 83, 2531–2541 (2015).

M. Nelson, S. K. Reddy, T. S. Ratliff, M. Z. Hossain, A. S. Katseff, A. S. Zhu, E. Chang, S. R. Resnik, C. Page, D. Kim, A. J. Whittam, L. S. Miller, L. A. Garza, dsRNA released by tissue damage activates TLR3 to drive skin regeneration. Cell Stem Cell 17, 139–151 (2015).

W. A. Boisvert, M. Yu, Y. Choi, G. H. Jeong, Y. L. Zhang, S. Cho, C. Choi, S. Lee, B. H. Lee, Hair growth-promoting effect of Geranium sibiricum extract in human dermal papilla cells and C57BL/6 mice. BMC Complement. Altern. Med. 17, 109 (2017).

M. Chai, M. Jiang, L. Vergnes, X. Fu, S. C. de Barros, N. B. Doan, W. Huang, J. Chu, J. Jiao, H. Herschman, G. M. Crooks, K. Reue, J. Huang, Stimulation of hair growth by small molecules that activate autophagy. Cell Rep. 27, 3413–3421.e3 (2019).

K. Allmeroth, C. S. Kim, A. Annibal, A. Pouikli, J. Koester, M. J. Derisbourg, C. Andre Chacon-Martinez, C. Latza, A. Antebi, P. Tessarz, S. A. Wickstrom, M. S. Denzel,

N1-acetylspermidine is a determinant of hair follicle stem cell fate. J. Cell Sci. 134, jcs252767 (2021).

S. Park, W. Kang, D. Choi, B. Son, T. Park, Nonanal stimulates growth factors via cyclic adenosine monophosphate (cAMP) signaling in human hair follicle dermal papilla cells. Int. J. Mol. Sci. 21, 8054 (2020).

G. Biolo, G. Toigo, B. Ciocchi, R. Situlin, F. Iscra, A. Gullo, G. Guarnieri, Metabolic response to injury and sepsis: Changes in protein metabolism. Nutrition 13, 52S–57S (1997).

U. Kesici, S. Kesici, H. Ulusoy, F. Yucesan, A. U. Turkmen, A. Besir, V. Tuna, Effects of glutamine on wound healing. Int. Wound J. 12, 280–284 (2015).

N. K. Archer, J. H. Jo, S. K. Lee, D. Kim, B. Smith, R. V. Ortines, Y. Wang, M. C. Marchitto, A. Ravipati, S. S. Cai, C. A. Dillen, H. Liu, R. J. Miller, A. G. Ashbaugh, A. S. Uppal, M. K. Oyoshi, N. Malhotra, S. Hoff, L. A. Garza, H. H. Kong, J. A. Segre, R. S. Geha, L. S. Miller, Injury, dysbiosis, and filaggrin deficiency drive skin inflammation through keratinocyte IL-1α release. J. Allergy Clin. Immunol. 143, 1426–1443.e6 (2019).

D. Kim, R. Chen, M. Sheu, N. Kim, S. Kim, N. Islam, E. M. Wier, G. Wang, A. Li, A. Park, W. Son, B. Evans, V. Yu, V. P. Prizmic, E. Oh, Z. Wang, J. Yu, W. Huang, N. K. Archer, Z. Hu, N. Clemetson, A. M. Nelson, A. Chien, G. A. Okoye, L. S. Miller, G. Ghiaur, S. Kang, J. W. Jones, M. A. Kane, L. A. Garza, Noncoding dsRNA induces retinoic acid synthesis to stimulate hair follicle regeneration via TLR3. Nat. Commun. 10, 2811 (2019).

S. Stegen, N. van Gastel, G. Eelen, B. Ghesquiere, F. D'Anna, B. Thienpont, J. Goveia, S. Torrekens, R. Van Looveren, F. P. Luyten, P. H. Maxwell, B. Wielockx, D. Lambrechts, S. M. Fendt, P. Carmeliet, G. Carmeliet, HIF-1α promotes glutamine-mediated redox homeostasis and glycogen-dependent bioenergetics to support postimplantation bone cellsurvival. Cell Metab. 23, 265–279 (2016).

R. C. Sun, N. C. Denko, Hypoxic regulation of glutamine metabolism through HIF1 and SIAH2 supports lipid synthesis that is necessary for tumor growth. Cell Metab. 19, 285–292 (2014).

Y. Kanai, B. Clemencon, A. Simonin, M. Leuenberger, M. Lochner, M. Weisstanner, M. A. Hediger, The SLC1 high-affnity glutamate and neutral amino acid transporter family. Mol. Aspects Med. 34, 108–120 (2013).

S. Abbasi, S. Sinha, E. Labit, N. L. Rosin, G. Yoon, W. Rahmani, A. Jaffer, N. Sharma, A. Hagner, P. Shah, R. Arora, J. Yoon, A. Islam, A. Uchida, C. K. Chang, J. A.

Stratton, R. W. Scott, F. M. V. Rossi, T. M. Underhill, J. Biernaskie, Distinct regulatory programs control the latent regenerative potential of dermal fibroblasts during wound healing. Cell Stem Cell 27, 396–412.e6 (2020).

D. Haensel, S. Jin, P. Sun, R. Cinco, M. Dragan, Q. Nguyen, Z. Cang, Y. Gong, R. Vu, A. L. MacLean, K. Kessenbrock, E. Gratton, Q. Nie, X. Dai, Defining epidermal basal cell states during skin homeostasis and wound healing using single-cell transcriptomics. Cell Rep. 30, 3932–3947.e6 (2020).

D. Gay, O. Kwon, Z. Zhang, M. Spata, M. V. Plikus, P. D. Holler, M. Ito, Z. Yang, E. Treffeisen, C. D. Kim, A. Nace, X. Zhang, S. Baratono, F. Wang, D. M. Ornitz, S. E. Millar, G. Cotsarelis, Fgf9 from dermal γδ T cells induces hair follicle neogenesis after wounding. Nat. Med. 19, 916–923 (2013).

M. Ito, Z. Yang, T. Andl, C. Cui, N. Kim, S. E. Millar, G. Cotsarelis, Wnt-dependent de novo hair follicle regeneration in adult mouse skin after wounding. Nature 447, 316–320 (2007).

A. Mohyeldin, T. Garzon-Muvdi, A. Quinones-Hinojosa, Oxygen in stem cell biology: A critical component of the stem cell niche. Cell Stem Cell 7, 150–161 (2010).

M. Ito, Y. Liu, Z. Yang, J. Nguyen, F. Liang, R. J. Morris, G. Cotsarelis, Stem cells in the hair follicle bulge contribute to wound repair but not to homeostasis of the epidermis. Nat. Med. 11, 1351–1354 (2005).

J. Zhang, X. C. He, W. G. Tong, T. Johnson, L. M. Wiedemann, Y. Mishina, J. Q. Feng, L. Li, Bone morphogenetic protein signaling inhibits hair follicle anagen induction by restricting epithelial stem/progenitor cell activation and expansion. Stem Cells 24, 2826–2839 (2006).

S. Joost, A. Zeisel, T. Jacob, X. Sun, G. La Manno, P. Lonnerberg, S. Linnarsson, M. Kasper, Single-cell transcriptomics reveals that differentiation and spatial signatures shape epidermal and hair follicle heterogeneity. Cell Syst. 3, 221–237.e9 (2016).

P. G. Noleto, J. P. E. Saut, I. M. Sheldon, Short communication: Glutamine modulates inflammatory responses to lipopolysaccharide in ex vivo bovine endometrium. J. Dairy Sci. 100, 2207–2212 (2017).

K. Ren, R. Dubner, Interactions between the immune and nervous systems in pain. Nat. Med. 16, 1267–1276 (2010).

E. D. Milligan, L. R. Watkins, Pathological and protective roles of glia in chronic pain. Nat. Rev. Neurosci. 10, 23–36 (2009).

D. C. C. Healey, J. Y. Cephus, S. M. Barone, N. U. Chowdhury, D. O. Dahunsi,

M. Z. Madden, X. Ye, X. Yu, K. Olszewski, K. Young, V. A. Gerriets, P. J. Siska, R. Dworski, J. Hemler, J. W. Locasale, M. V. Poyurovsky, R. S. Peebles Jr., J. M. Irish, D. C. Newcomb, J. C. Rathmell, Targeting *in vivo* metabolic vulnerabilities of TH2 and TH17 cells reduces airway inflammation. J. Immunol. 206, 1127–1139 (2021).

G. Gao, C. Li, J. Zhu, Y. Wang, Y. Huang, S. Zhao, S. Sheng, Y. Song, C. Ji, C. Li, X. Yang, L. Ye, X. Qi, Y. Zhang, X. Xia, J. C. Zheng, Glutaminase 1 regulates neuroinflammation after cerebral ischemia through enhancing microglial activation and pro-inflammatory exosome release. Front. Immunol. 11, 161 (2020).

H. Morinaga, Y. Mohri, M. Grachtchouk, K. Asakawa, H. Matsumura, M. Oshima, N. Takayama, T. Kato, Y. Nishimori, Y. Sorimachi, K. Takubo, T. Suganami, A. Iwama, Y. Iwakura, A. A. Dlugosz, E. K. Nishimura, Obesity accelerates hair thinning by stem cell-centric converging mechanisms. Nature 595, 266–271 (2021).

P. Lee, R. Gund, A. Dutta, N. Pincha, I. Rana, S. Ghosh, D. Witherden, E. Kandyba, A. MacLeod, K. Kobielak, W. L. Havran, C. Jamora, Stimulation of hair follicle stem cell proliferation through an IL-1 dependent activation of γδT-cells. eLife 6, e28875 (2017).

L. Gong, J. Xiao, X. Li, Y. Li, X. Gao, X. Xu, IL-36α promoted wound induced hair follicle neogenesis via hair follicle stem/progenitor cell proliferation. Front. Cell Dev. Biol. 8, 627 (2020).

G. Wang, Y. Miao, N. Kim, E. Sweren, S. Kang, Z. Hu, L. A. Garza, Association of the psoriatic microenvironment with treatment response. JAMA Dermatol. 156, 1057–1065 (2020).

D. Zeng, Z. Ye, R. Shen, G. Yu, J. Wu, Y. Xiong, R. Zhou, W. Qiu, N. Huang, L. Sun, X. Li, J. Bin, Y. Liao, M. Shi, W. Liao, IOBR: Multiomics immunooncology biological research to decode tumor microenvironment and signatures. Front. Immunol. 12, 687975 (2021).

S. Jin, C. F. Guerrero-Juarez, L. Zhang, I. Chang, R. Ramos, C. H. Kuan, P. Myung, M. V. Plikus, Q. Nie, Inference and analysis of cell-cell communication using CellChat. Nat. Commun. 12, 1088 (2021).

Although the foregoing subject matter has been described in some detail by way of illustration and example for purposes of clarity of understanding, it will be understood by those skilled in the art that certain changes and modifications can be practiced within the scope of the appended claims.

THAT WHICH IS CLAIMED:

1. A method for promoting wound healing, treating photoaging, and/or inducing hair follicle regeneration, the method comprising administering to a subject in need of treatment thereof, a therapeutically effective amount of one or more bacteria and/or one or more dsRNA sufficient to promote wound healing, treat photoaging, and/or induce hair follicle regeneration in the subject.

2. The method of claim 1, wherein the one or more bacteria are selected from *Staphylococcus*, *Pseudomonas*, and *Streptococcus*.

3. The method of claim 2, wherein the one or more bacteria are *S. aureus*.

4. The method of any one of claims 1 to 3, wherein administration of the one or more bacteria and/or one or more dsRNA:

(a) induces local hypoxia and activates HIF1α signaling;

(b) induces glutamine metabolism in one or more keratinocytes; and/or

(c) activates downstream IL-1β signaling.

5. The method of any one of claims 1 to 4, wherein the one or more bacteria and/or one of more dsRNA are applied topically to the wound and/or an area surrounding the wound.

6. The method of any one of claims 1 to 5, wherein the wound is selected from a poor healing wound, a chronic wound, a diabetic chronic wound, a venous stasis chronic wound, an incised wound, and a tearing wound.

7. The method of any one of claims 1 to 6, wherein the one or more bacteria and/or one or more dsRNA are administered via a pharmaceutical formulation.

8. The method of claim 7, wherein the pharmaceutical formulation comprises one or more of a solvent/liquid carrier, an emulsion, a cream, an ointment, a gel, a solid excipient, a polymer-based carrier, a liposome-based carrier, and a nanoparticle or microparticle.

9. The method of claim 7, wherein the pharmaceutical formulation comprises a bandage or a gauze.

10. The method of claim 7, wherein the pharmaceutical formulation further comprises one or more additional agents for promoting wound healing, treating photoaging, and/or inducing hair follicle regeneration.

11. The method of claim 10, wherein the one or more additional agents are selected from a retinoid, a vitamin, an anti-inflammatory agent, a steroid, a natural product, an antioxidant, and an analgesic.

12. A method for promoting wound healing, treating photoaging, and/or inducing hair follicle regeneration, the method comprising administering to a subject in need of treatment thereof, a therapeutically effective amount of glutamine and/or glutamate with or without one or more dsRNA sufficient to promote wound healing, treat photoaging, and/or induce hair follicle regeneration in the subject.

13. The method of claim 12, wherein administration of the glutamine and/or glutamate with or without one or more dsRNA:

(a) induces local hypoxia and activates HIF1α signaling;

(b) induces glutamine metabolism in one or more keratinocytes; and/or

(c) activates downstream IL-1β signaling.

14. The method of any one of claims 12 to 13, wherein the glutamine and/or glutamate with or without one or more dsRNA are applied topically to the wound and/or an

area surrounding the wound.

15. The method of any one of claims 12 to 14, wherein the wound is selected from a poor healing wound, a chronic wound, a diabetic chronic wound, a venous stasis chronic wound, an incised wound, and a tearing wound.

16. The method of any one of claims 12 to 15, wherein the glutamine and/or glutamate with or without one or more dsRNA are administered via a pharmaceutical formulation.

17. The method of claim 16, wherein the pharmaceutical formulation comprises one or more of a solvent/liquid carrier, an emulsion, a cream, an ointment, a gel, a solid excipient, a polymer-based carrier, a liposome-based carrier, and a nanoparticle or microparticle.

18. The method of claim 17, wherein the pharmaceutical formulation comprises a bandage or a gauze.

19. The method of claim 17, wherein the pharmaceutical formulation further comprises one or more additional agents for promoting wound healing, treating photoaging, and/or inducing hair follicle regeneration.

20. The method of claim 17, wherein the one or more additional agents are selected from a retinoid, a vitamin, an anti-inflammatory agent, a steroid, a natural product, an antioxidant, and an analgesic.

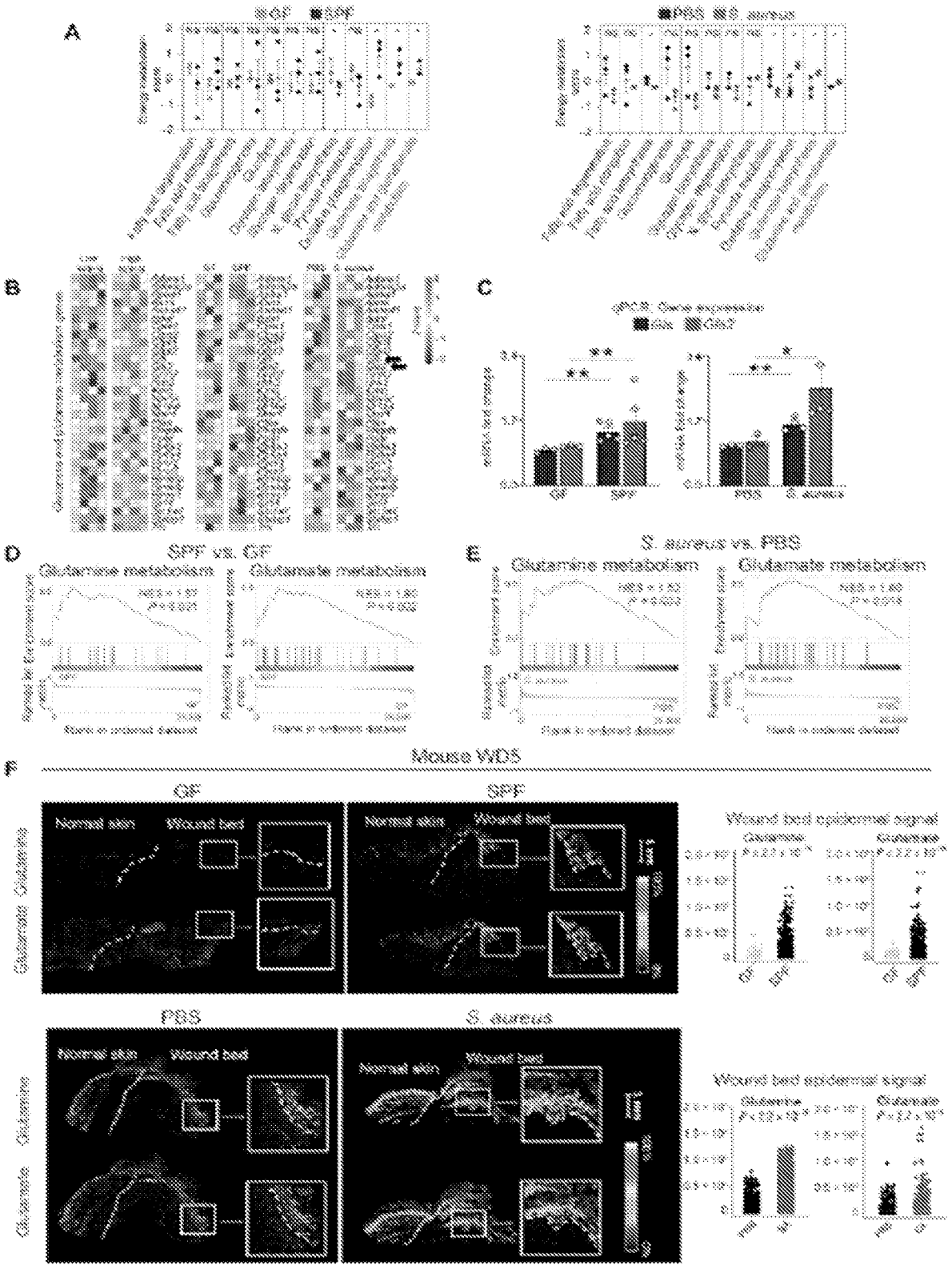
A
GF
SPF
PBS
S. aureus
B
C
D
SPF vs. GF
Glutamine metabolism
Glutamate metabolism
E
S. aureus vs. PBS
Glutamine metabolism
Glutamate metabolism
F
Mouse WDS
GF
SPF
PBS
S. aureus
Normal skin
Wound bed
Wound bed epidermal signal
Glutamine
Glutamate

Fig. 1

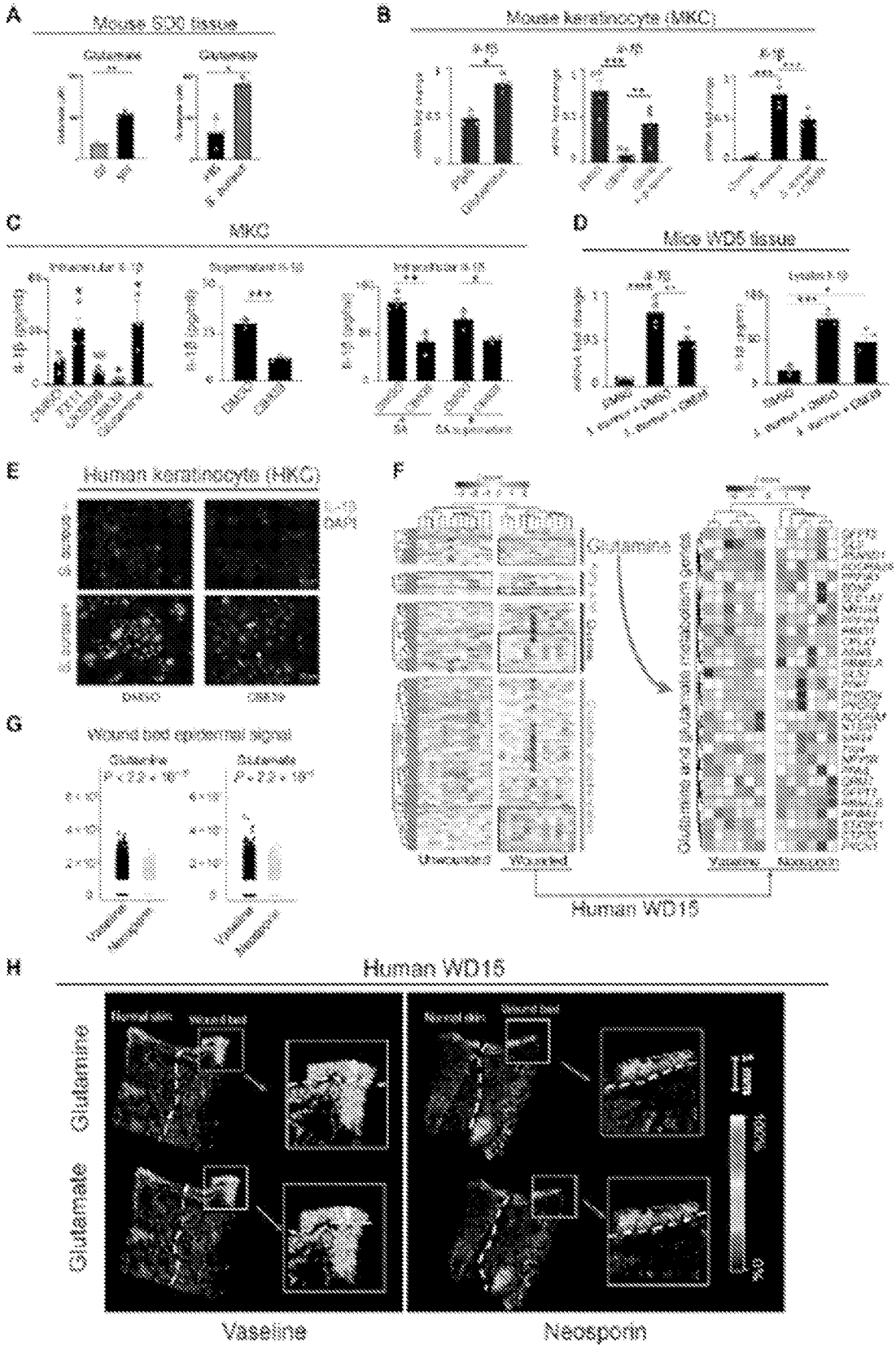
A
Mouse S2R tissue
B
Mouse keratinocyte (MKC)
C
MKC
D
Mice WD5 tissue
E
Human keratinocyte (HKC)
F
Human WD15
G
H
Human WD15
Glutamine
Glutamate
Vaseline
Neosporin

Fig. 2

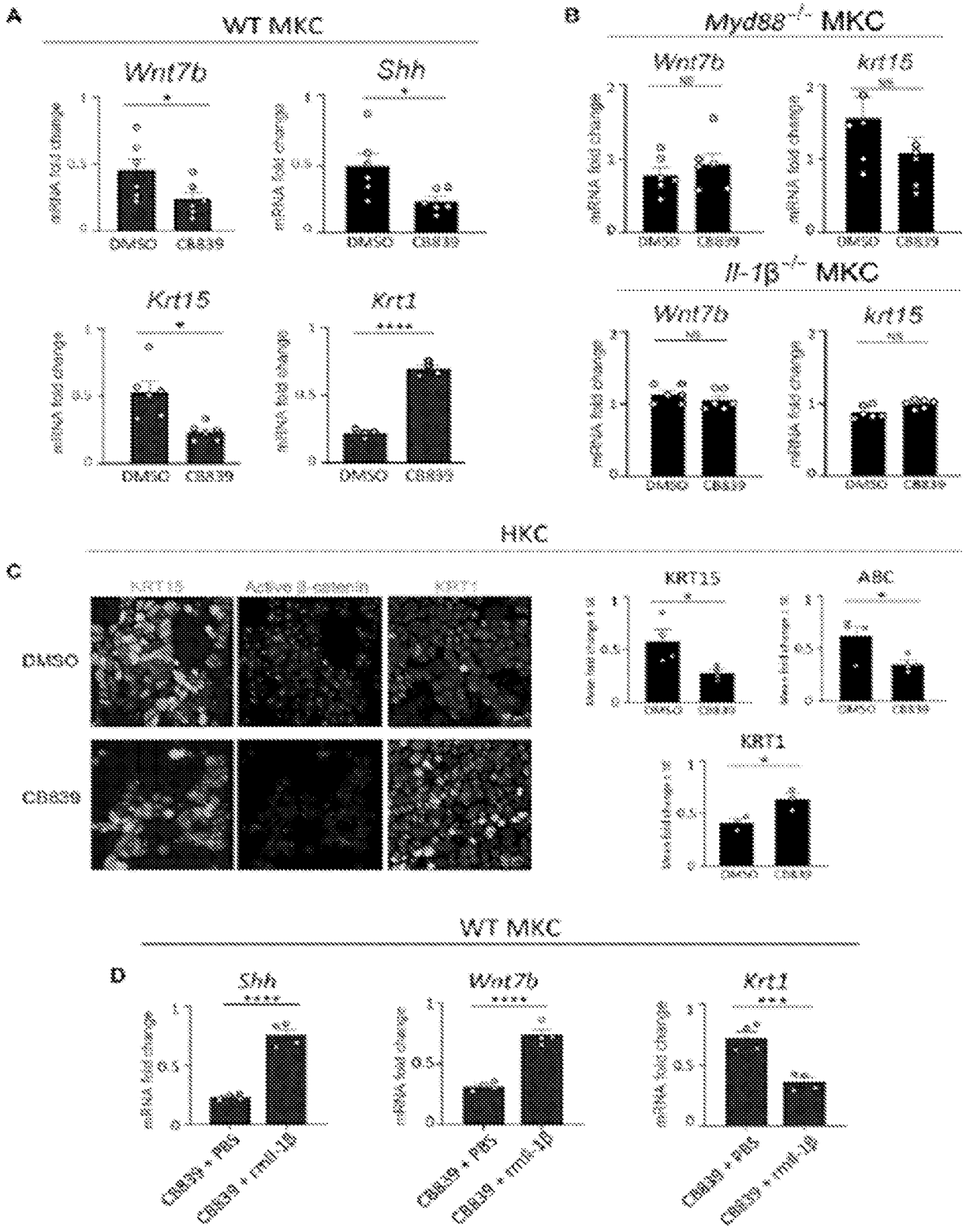
A
WT MKC
Wnt7b
Shh
Krt15
Krt1
DMSO
CB839
B
Myd88−/− MKC
Il-1β−/− MKC
Wnt7b
krt15
C
HKC
DMSO
CB839
KRT15
ABC
KRT1
D
WT MKC
Shh
Wnt7b
Krt1
CB839 + PBS
CB839 + rmIL-1β

Fig. 3

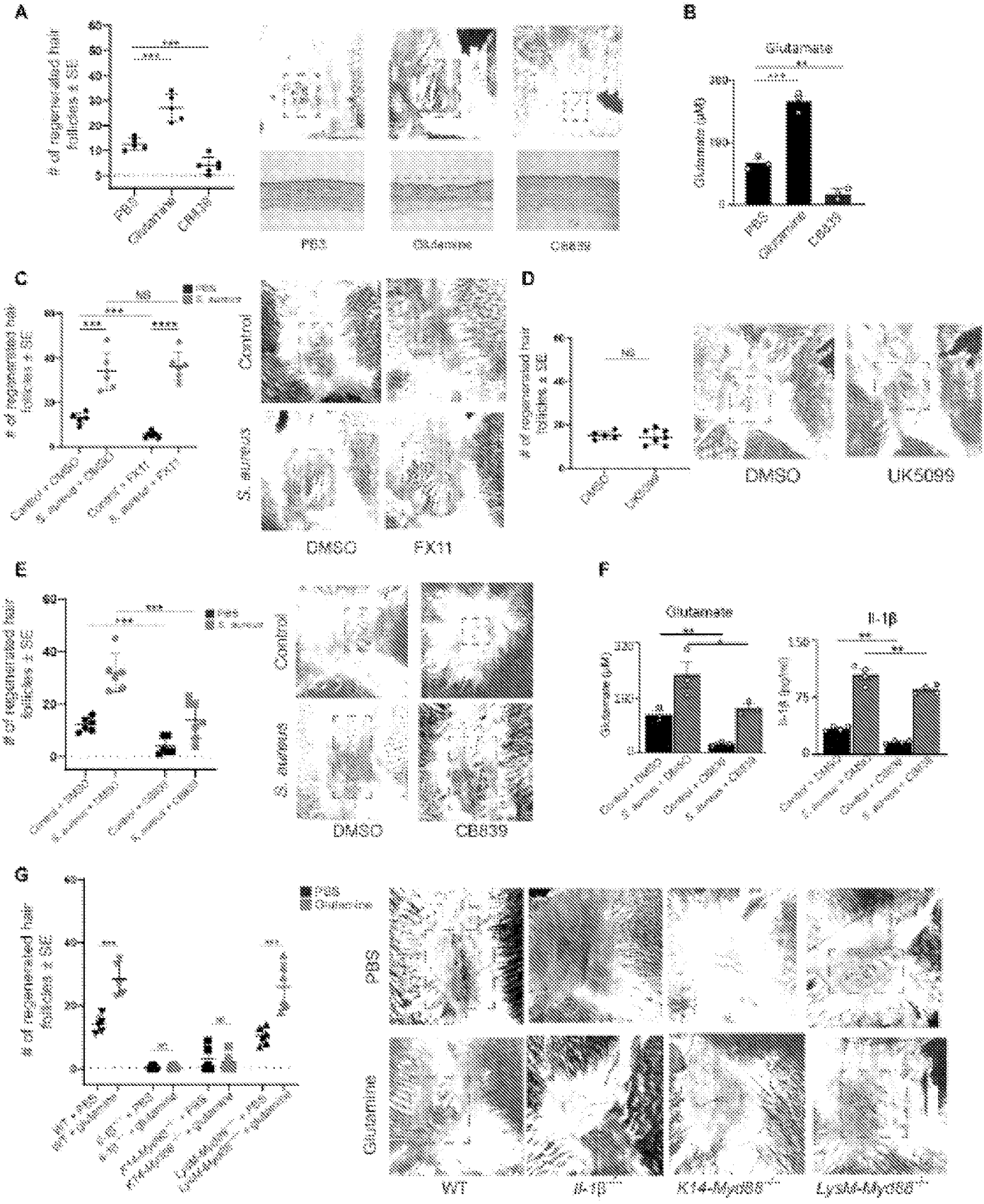
A
B
C
D
E
F
G
PBS
Glutamine
Control
S. aureus
DMSO
FX11
UK5099
CB839
WT
IL-1β-/-
K14-MyD88-/-
LysM-MyD88-/-

Fig. 4

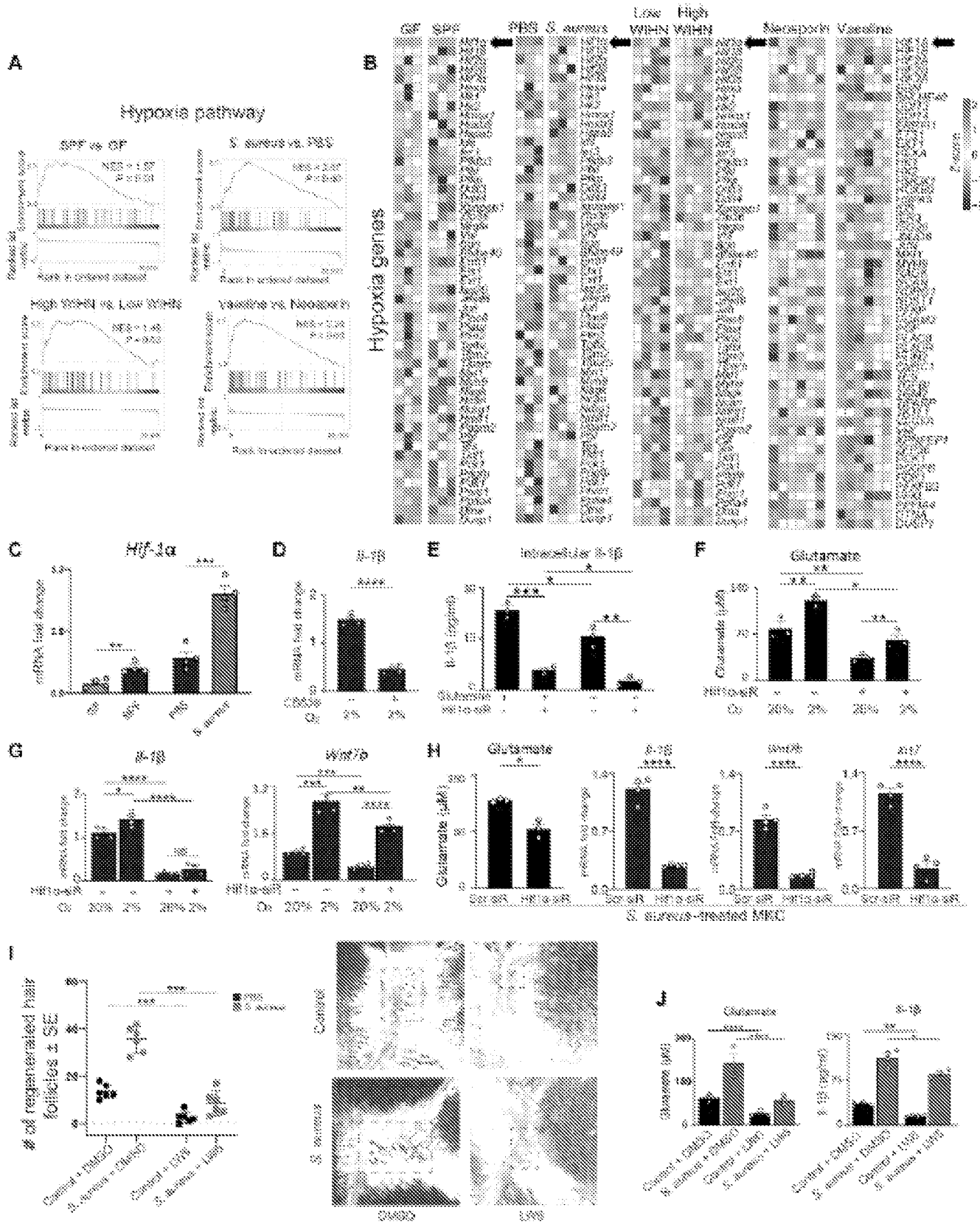
A
Hypoxia pathway
SPF vs. GF
S. aureus vs. PBS
High WIHN vs. Low WIHN
Vaseline vs. Neosporin
B
GF
SPF
PBS
S. aureus
Low WIHN
High WIHN
Neosporin
Vaseline
Hypoxia genes
C
Hif-1α
D
IL-1β
E
Intracellular IL-1β
F
Glutamate
G
IL-1β
Wnt7b
H
Glutamate
IL-1β
Wnt7b
Axin2
S. aureus-treated MEC
I
# of regenerated hair follicles ± SE
Control + DMSO
S. aureus + DMSO
Control + LiCl
S. aureus + LiCl
Control
S. aureus
DMSO
LiCl
J
Glutamate
IL-1β
Control + DMSO
S. aureus + DMSO
Control + LiCl
S. aureus + LiCl

Fig. 5

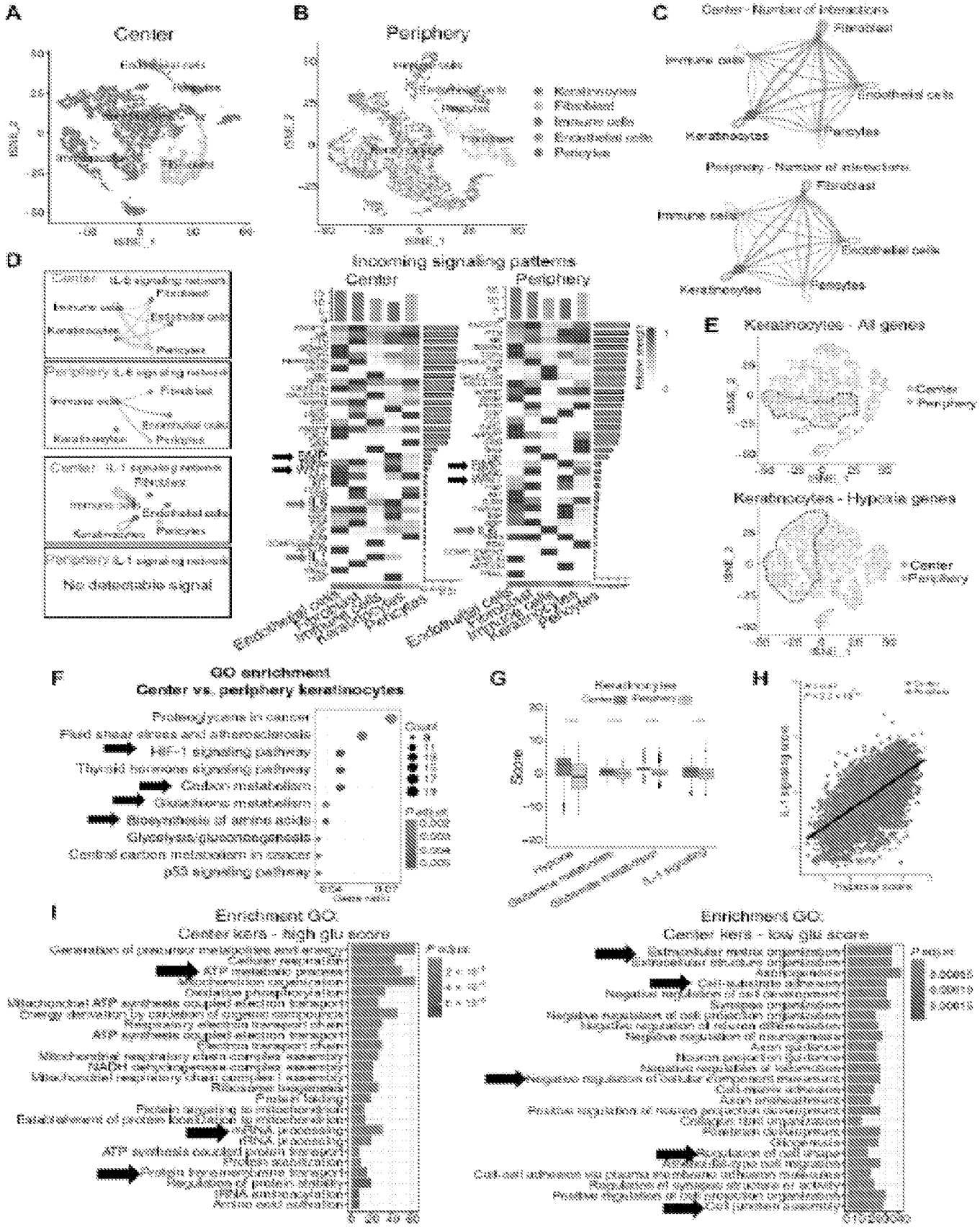
A
Center
B
Periphery
C
Center - Number of interactions
Periphery - Number of interactions
Fibroblast
Immune cells
Endothelial cells
Keratinocytes
Pericytes
D
Incoming signaling patterns
Center
Periphery
IL6 signaling network
No detectable signal
E
Keratinocytes - All genes
Keratinocytes - Hypoxia genes
F
GO enrichment
Center vs. periphery keratinocytes
Proteoglycans in cancer
Fluid shear stress and atherosclerosis
HIF-1 signaling pathway
Thyroid hormone signaling pathway
Carbon metabolism
Glutathione metabolism
Biosynthesis of amino acids
Glycolysis/gluconeogenesis
Central carbon metabolism in cancer
p53 signaling pathway
G
Keratinocytes
Score
Hypoxia
Glycolysis metabolism
Citrulline metabolism
IL6 signaling
H
IL6 signaling score
Hypoxia score
I
Enrichment GO:
Center kers - high glu score
Enrichment GO:
Center kers - low glu score

Fig. 6

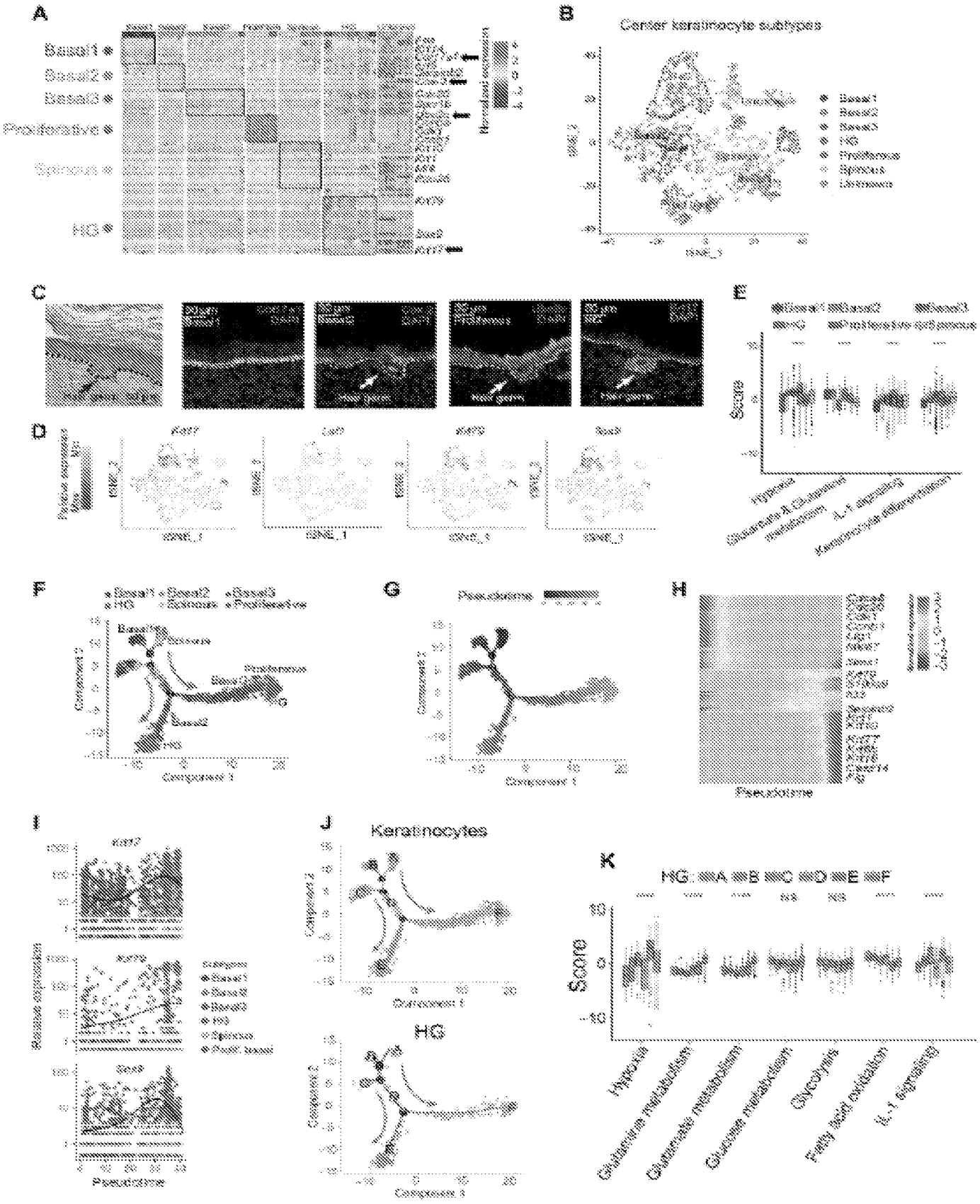
A
Basal1
Basal2
Basal3
Proliferative
Spinous
HG
Normalized enrichment
B
Cancer keratinocyte subtypes
Basal1
Basal2
Basal3
HG
Proliferative
Spinous
Differentiated
C
D
Krt7
Cst3
Krt79
Sox9
Relative expression
E
Score
Hypoxia
Glutamine & Glutathione metabolism
IL-1 signaling
Keratinocyte differentiation
F
Component 1
Component 2
G
Pseudotime
H
Pseudotime
I
Krt7
Krt79
Sox9
Relative expression
Pseudotime
J
Keratinocytes
HG
K
HG: A B C D E F
Score
Hypoxia
Glutamine metabolism
Glutamate metabolism
Glucose metabolism
Glycolysis
Fatty acid oxidation
IL-1 signaling

Fig. 7

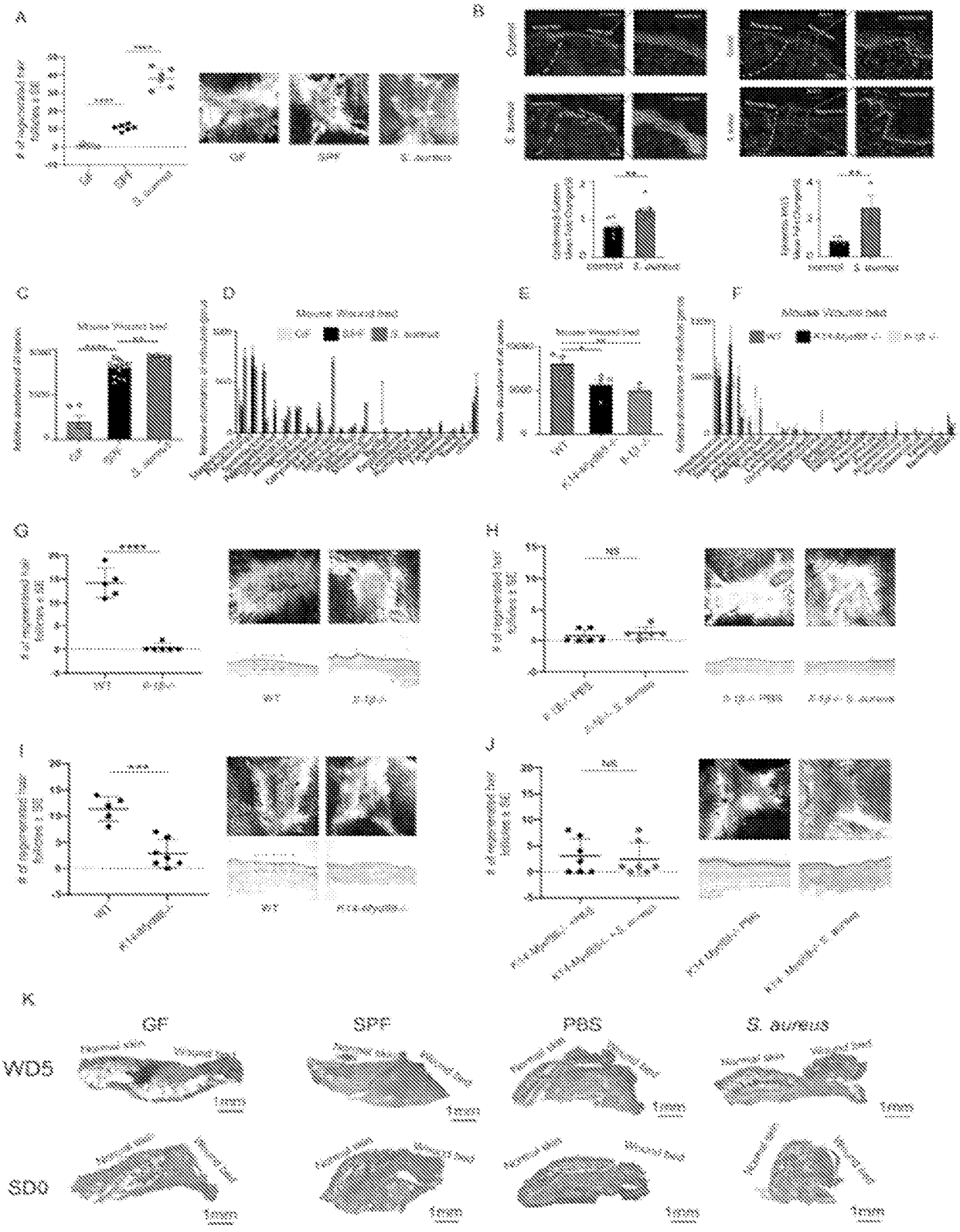

Fig. 8

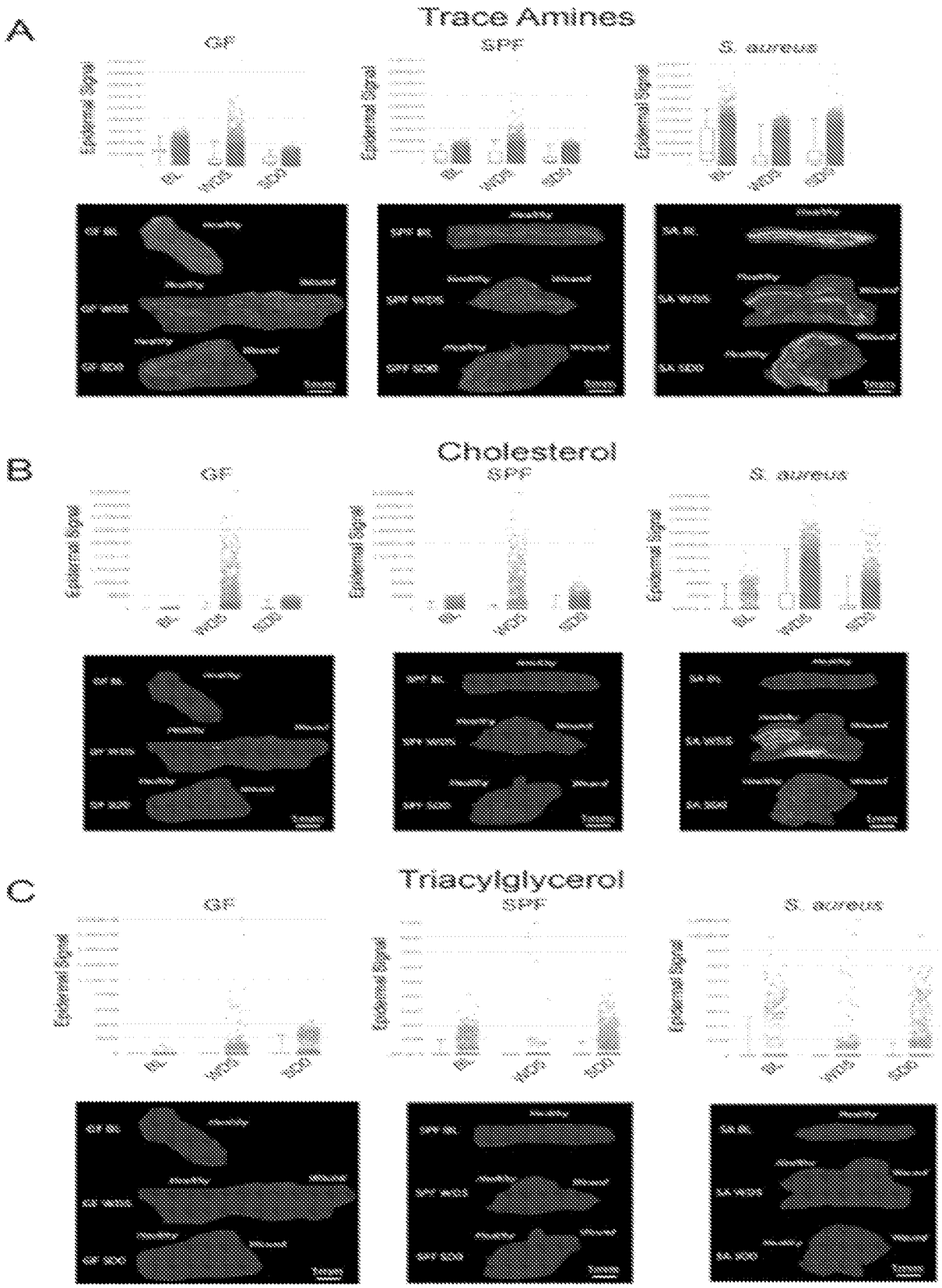
A
Trace Amines
GF
SPF
S. aureus
Colonial Signal
B
Cholesterol
GF
SPF
S. aureus
Colonial Signal
C
Triacylglycerol
GF
SPF
S. aureus
Colonial Signal

Fig. 9

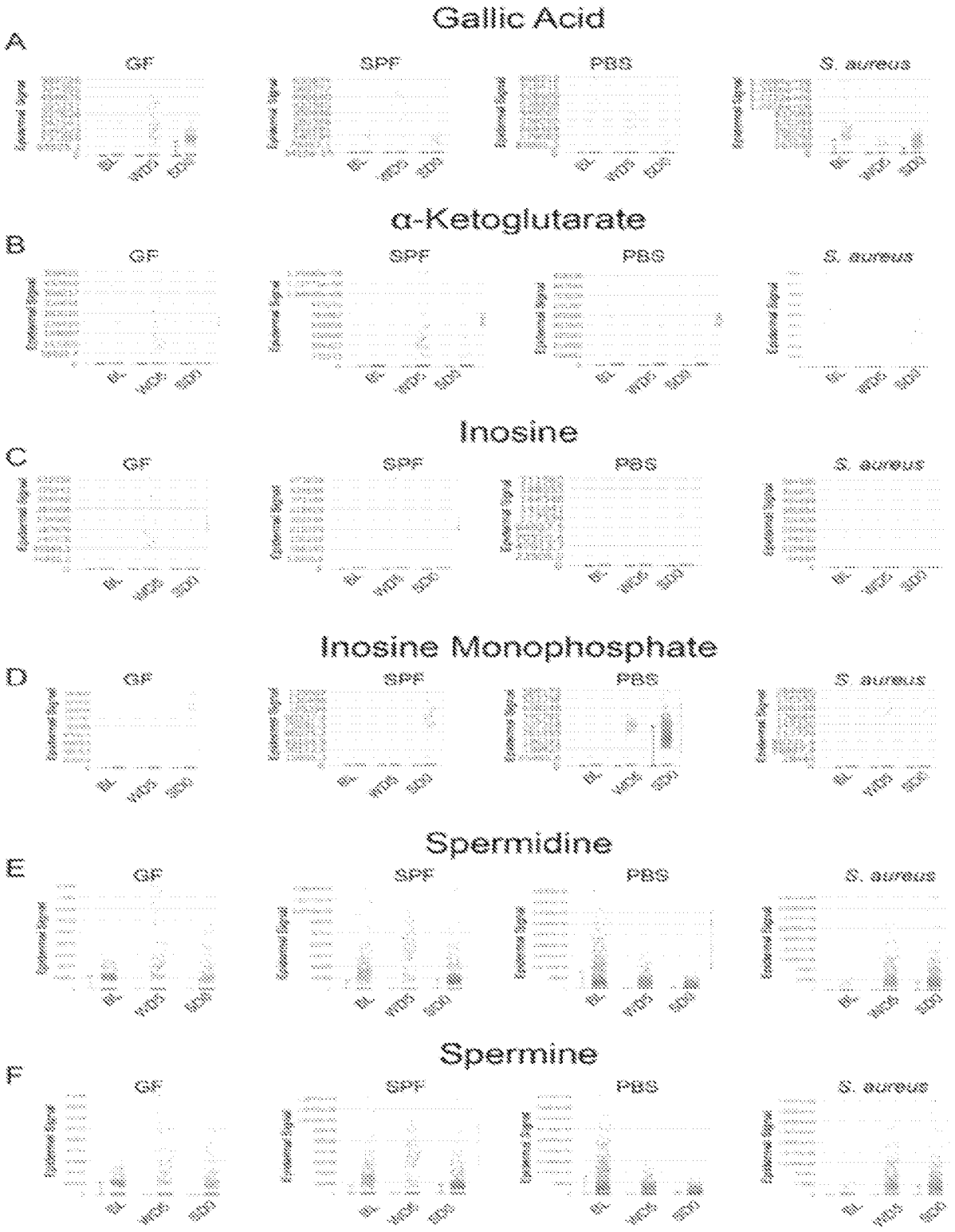
A
Gallic Acid
GF
SPF
PBS
S. aureus
B
α-Ketoglutarate
C
Inosine
D
Inosine Monophosphate
E
Spermidine
F
Spermine

Fig. 10

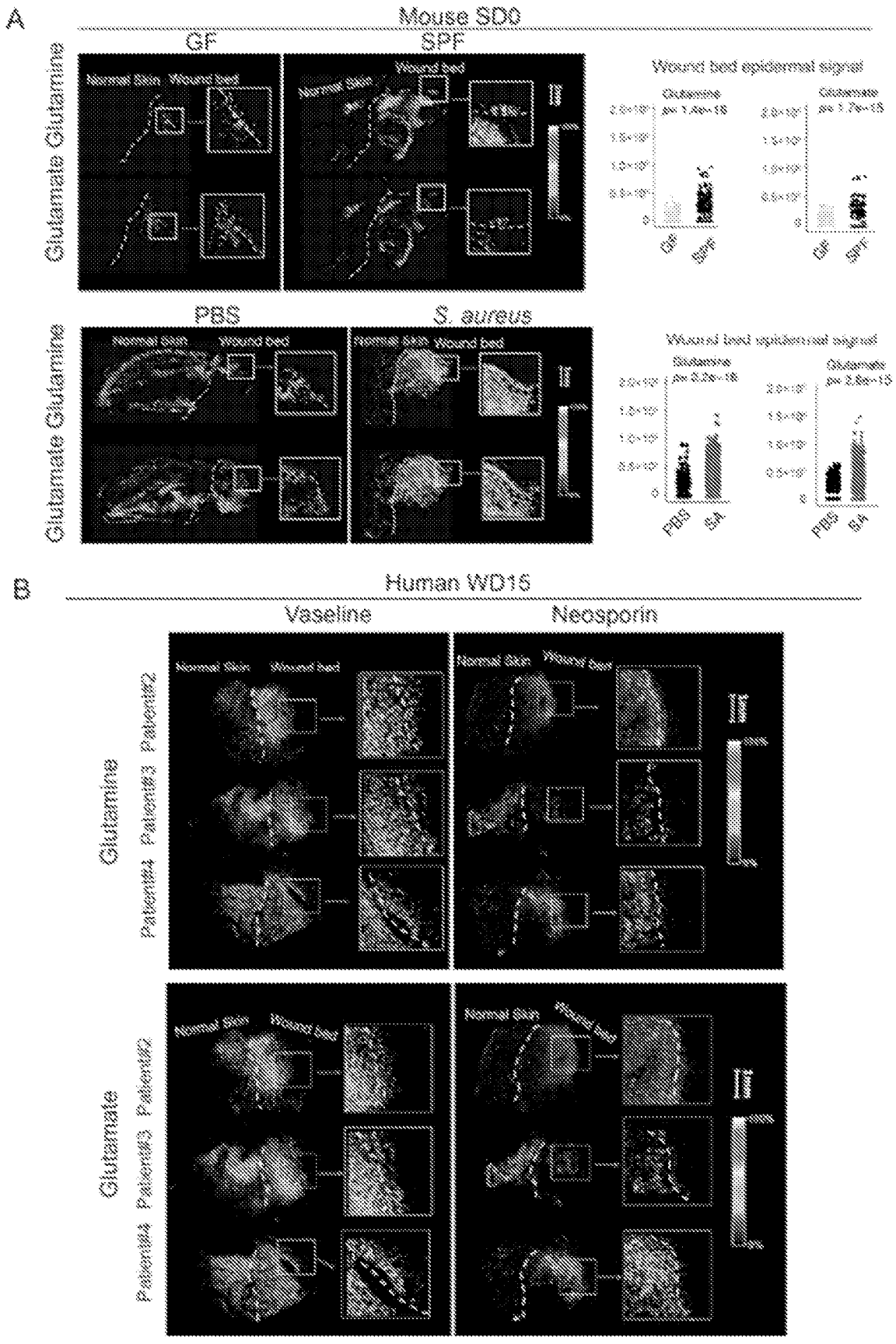
A
Mouse SD0
GF
SPF
Glutamate Glutamine
Normal Skin
Wound bed
Wound bed epidermal signal
Glutamine
Glutamate
PBS
S. aureus
B
Human WD15
Vaseline
Neosporin
Glutamine
Glutamate
Patient#2
Patient#3
Patient#4

Fig. 11

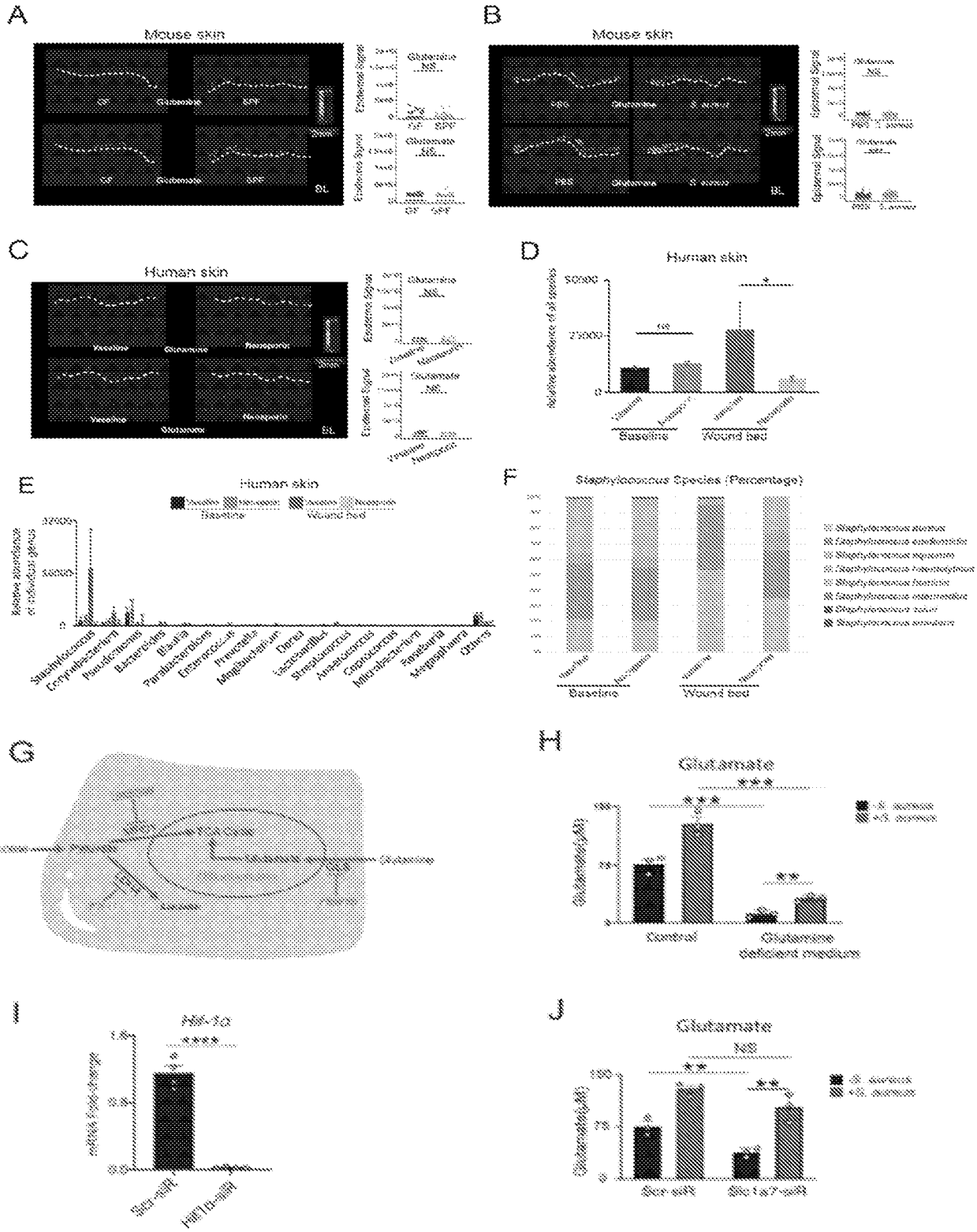
A
Mouse skin
Glutamate
B
Mouse skin
Glutamate
C
Human skin
Glutamate
D
Human skin
Baseline
Wound bed
E
Human skin
Baseline
Wound bed
F
Staphylococcus Species (Percentage)
Baseline
Wound bed
G
H
Glutamate
Control
Glutamine deficient medium
I
Atk-1α
Skin-cell
Hair follicle-cell
J
Glutamate
Skin cell
Skin cancer cell

Fig. 12

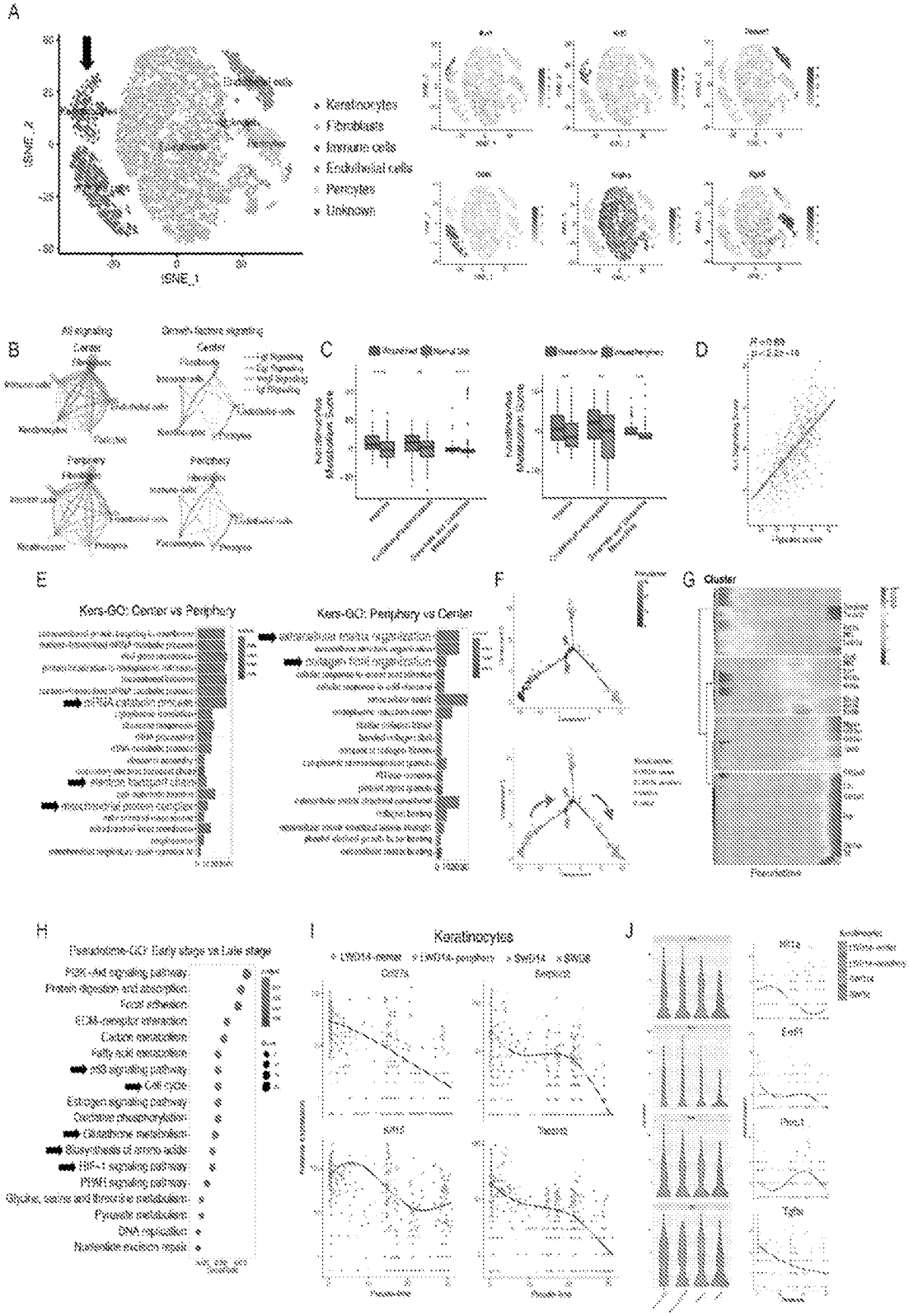
A
Keratinocytes
Fibroblasts
Immune cells
Endothelial cells
Pericytes
Unknown
tSNE_1
tSNE_2
B
Center
Periphery
C
D
E
Kers-GC: Center vs Periphery
Kers-GC: Periphery vs Center
F
G
Cluster
H
Pseudotime-GO: Early stage vs Late stage
I
Keratinocytes
J

Fig. 13

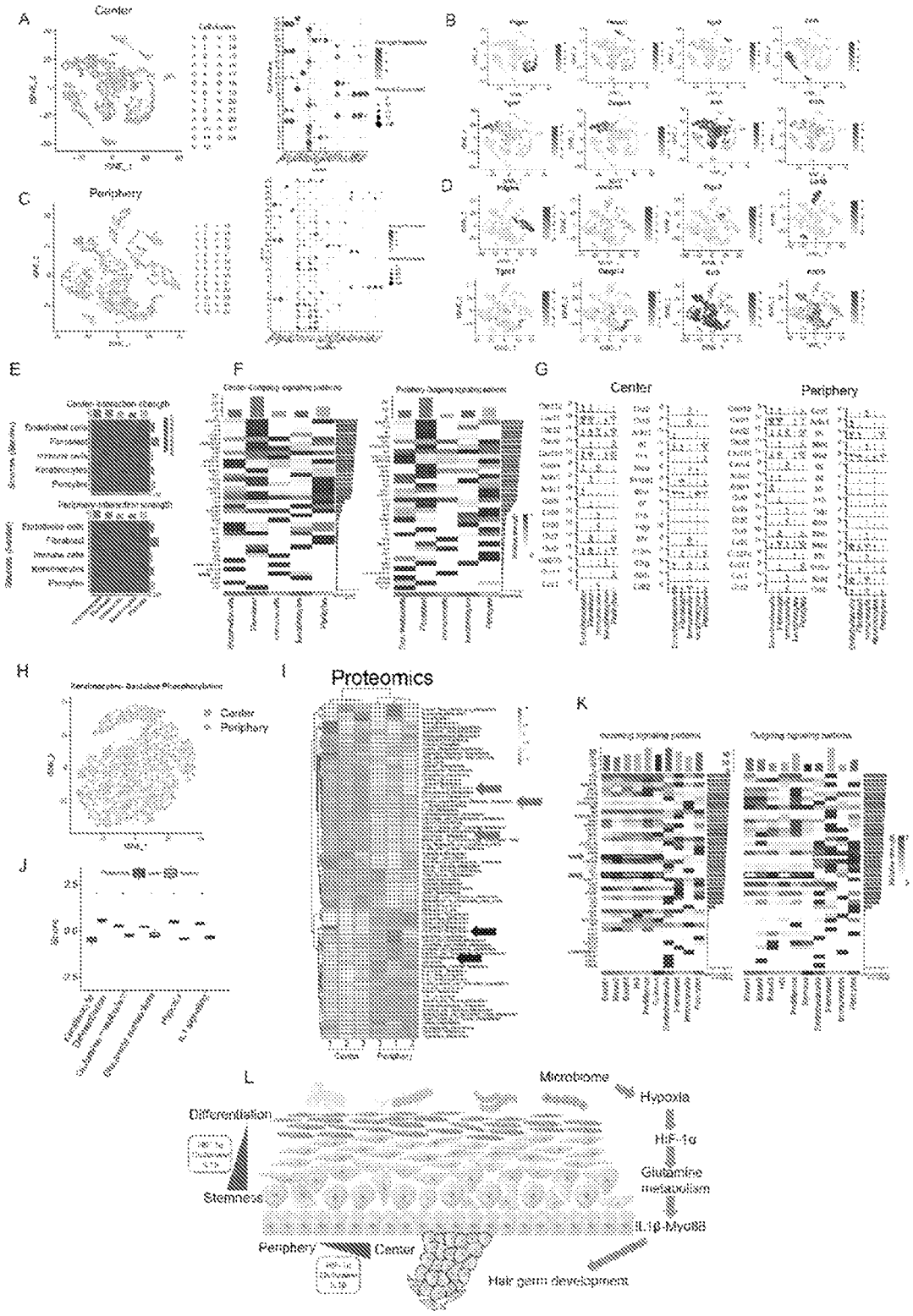
A
Center
B
C
Periphery
D
E
F
G
Center
Periphery
H
Center
Periphery
I
Proteomics
J
K
L
Microbiome
Hypoxia
HIF-1α
Glutamine metabolism
IL1β-Myd88
Differentiation
Stemness
Periphery
Center
Hair germ development

Fig. 14

INTERNATIONAL SEARCH REPORT

International application No.
PCT/US2024/058629

A. CLASSIFICATION OF SUBJECT MATTER

IPC: ***C12N 15/113*** (2025.01); ***A61K 35/741*** (2025.01); ***A61K 31/7088*** (2025.01); ***A61P 17/02*** (2025.01); *A61K 31/223* (2025.01); *A61K 35/74* (2025.01)

CPC: ***C12N 15/113; A61K 35/741; A61K 31/7088; A61P 17/02;*** *A61K 31/223; A23L 33/135; A61K 38/2006*

According to International Patent Classification (IPC) or to both national classification and IPC

B. FIELDS SEARCHED

Minimum documentation searched (classification system followed by classification symbols)

See Search History Document

Documentation searched other than minimum documentation to the extent that such documents are included in the fields searched

See Search History Document

Electronic data base consulted during the international search (name of data base and, where practicable, search terms used)

See Search History Document

C. DOCUMENTS CONSIDERED TO BE RELEVANT

Category*	Citation of document, with indication, where appropriate, of the relevant passages	Relevant to claim No.
X	WANG et al. "Commensal microbiome promotes hair follicle regeneration by inducing keratinocyte HIF-1a signaling and glutamine metabolism" Sci. Adv. 4 January 2023, Vol. 9, eabo7555, pp. 1-17 abstract, pg 2, col 1, para 3, pg 2, col 2, para 2, pg 5, col 2, para 1, pg 14, col 1, para 3	1-4, 12-14
A	LAN et al. "dsRNA Induced IFNß-MMP13 Axis Drives Corneal Wound Healing" Invest Ophthalmol Vis Sci. 2022; Vol. 63, No. 2, Article 14, pp. 1-11 abstract, pg. 9, col 2, para 1	1
A	PENG et al. "LncRNA GAS5 activates the HIF1A/VEGF pathway by binding to TAF15 to promote wound healing in diabetic foot ulcers" Laboratory Investigation, 2021, Vol. 101, pp. 1071-1083 abstract, pg 1075, col 2, para 1, pg 1077, col 2, para 1	1

☐ Further documents are listed in the continuation of Box C. ☐ See patent family annex.

* Special categories of cited documents:
"A" document defining the general state of the art which is not considered to be of particular relevance
"D" document cited by the applicant in the international application
"E" earlier application or patent but published on or after the international filing date
"L" document which may throw doubts on priority claim(s) or which is cited to establish the publication date of another citation or other special reason (as specified)
"O" document referring to an oral disclosure, use, exhibition or other means
"P" document published prior to the international filing date but later than the priority date claimed
"T" later document published after the international filing date or priority date and not in conflict with the application but cited to understand the principle or theory underlying the invention
"X" document of particular relevance; the claimed invention cannot be considered novel or cannot be considered to involve an inventive step when the document is taken alone
"Y" document of particular relevance; the claimed invention cannot be considered to involve an inventive step when the document is combined with one or more other such documents, such combination being obvious to a person skilled in the art
"&" document member of the same patent family

Date of the actual completion of the international search	Date of mailing of the international search report
11 January 2025 (11.01.2025)	**23 January 2025 (23.01.2025)**

Name and mailing address of the ISA/US	Authorized officer
COMMISSIONER FOR PATENTS **MAIL STOP PCT, ATTN: ISA/US** **P.O. Box 1450** **Alexandria, VA 22313-1450** **UNITED STATES OF AMERICA**	**KARI RODRIQUEZ**
Facsimile No. **571-273-8300**	Telephone No. **PCT Help Desk: 571-272-4300**

INTERNATIONAL SEARCH REPORT

International application No.
PCT/US2024/058629

Box No. II Observations where certain claims were found unsearchable (Continuation of item 2 of first sheet)

This international search report has not been established in respect of certain claims under Article 17(2)(a) for the following reasons:

1. ☐ Claims Nos.:
because they relate to subject matter not required to be searched by this Authority, namely:

2. ☐ Claims Nos.:
because they relate to parts of the international application that do not comply with the prescribed requirements to such an extent that no meaningful international search can be carried out, specifically:

3. ☑ Claims Nos.: **5-11, 15-20**
because they are dependent claims and are not drafted in accordance with the second and third sentences of Rule 6.4(a).